THE PENNSYLVANIA STATE UNIVERSITY
SCHREYER HONORS COLLEGE

DEPARTMENT OF MECHANICAL & NUCLEAR ENGINEERING

VEHICLE PATH FOLLOWING AND ROLLOVER PREVENTION USING PREVIEWED STATE INFORMATION

PAUL STANKIEWICZ
Spring 2013

A thesis
submitted in partial fulfillment
of the requirements
for a baccalaureate degree
in Mechanical Engineering
with honors in Mechanical Engineering

Reviewed and approved* by the following:

Dr. Sean Brennan
Associate Professor of Mechanical Engineering
Thesis Supervisor

Dr. H. J. Sommer III
Professor of Mechanical Engineering
Honors Advisor

* Signatures are on file in the Schreyer Honors College.

We approve the thesis of Paul Stankiewicz:

Date of Signature

Dr. Sean Brennan
Associate Professor of Mechanical Engineering
Thesis Supervisor

Dr. H. J. Sommer III
Professor of Mechanical Engineering
Honors Advisor

ABSTRACT

The research in this thesis focuses on investigating methods of vehicle path following and rollover prevention with application towards autonomous vehicles. Statistics show that although rollover only occurs in 2.2% of total highway crashes, it accounts for 10.7% of total fatalities. Autonomous vehicles must be able to remain within the bounds of the road, while also preventing rollover during emergency situations. Vehicle path following is a mature problem and has been investigated several ways, one of which will be used and evaluated in this research. There are also several dynamic rollover metrics in use that measure a vehicle's rollover propensity under specified conditions. However, in order to prevent a rollover event from occurring, it is necessary to predict a vehicle's rollover propensity in the future. This research uses a novel vehicle rollover metric, called the zero-moment point (ZMP), to predict the vehicle's rollover propensity. Comparing different amounts of preview, the results show that short-range predictions - as little as 0.75 seconds ahead of the vehicle - are sufficient to prevent nearly all dynamics-induced rollovers in typical shoulders and medians.

Table of Contents

List of Figures

List of Tables

Acknowledgements

I would first like to thank Dr. Brennan for his guidance in my work on this thesis. He has been an excellent adviser throughout my undergraduate work, especially in his advice for this thesis. He has taken the time to answer my questions and help me work through my problems even while on sabbatical in Australia. I look forward to working with him in the future in graduate school.

I would also like to thank Alex Brown for his invaluable help in the research for this thesis. He taught me many of the advanced concepts necessary to begin and complete this research. Needless to say, I would have been completely lost on several occasions without his help.

Finally, thanks to Dr. Sommer for taking the time to review my thesis and thanks to the Department of Mechanical and Nuclear Engineering for providing the resources I needed to conduct this research.

Chapter 1 - Literature Review

1.1 Introduction

Safety has long been recognized as one of the most important considerations in automobile design. Although modern cars have made driving a mundane activity, many drivers tend to forget the inherent danger of traveling in an automobile at high speeds. Over 5.5 million crashes were reported by the National Highway Traffic Safety Administration (NHTSA) [1] in the United States in 2009. Almost 31,000 of these crashes were fatal. While this number has steadily decreased by 14% since 2005, it is still an unacceptable statistic. The emergence of autonomous vehicles in the near future demands reliable safety systems that are capable of protecting occupants without direct driver intervention.

The concern over automobile safety has led to the implementation of many design features such as air bags, restraints, etc. The NHTSA estimated that in the past 35 years, over 350,000 lives have been saved due to these safety features [1]. In the hopes of further increasing this number, there has been ongoing research on vehicle safety systems, particularly regarding vehicle rollover. Vehicle rollover remains one of the deadliest types of automobile accident. Although rollover occurred in only 2.2% of total crashes, it accounted for 10.7% of total fatalities [1]. Vans, trucks, and SUVs are especially prone to rollover due to their high center of gravity. Therefore, investigating the roll stability of a vehicle is important in improving overall safety.

Much of the current research regarding vehicle rollover aims to measure or predict a vehicle's rollover propensity. The most explicit method of determining rollover propensity is full-scale vehicle testing. This method permits the vehicle to be driven through a test suite of worst-case maneuvers to characterize potential rollover. However, full-scale testing is expensive and incomplete; it is impossible to recreate all possible driving situations when considering the road trajectory, vehicle speed, variations in terrain, weather conditions, and possible obstacles in the road.

Alternatively, research is also being performed to measure rollover propensity by establishing metrics that quantify the onset of rollover. Several variations of rollover metrics exist including static or steady-state metrics, dynamic metrics, metrics utilizing the knowledge of ground-vehicle forces, and metrics considering the vehicle's states. A commonly used static metric is known as the Static Stability Factor (SSF) [2]. The SSF is an important factor in the NHTSA's five-star rating system for vehicle rollover, which combines SSF values with crash data for the particular vehicle. The SSF can be viewed as the lateral acceleration necessary for rollover to occur on a flat road during a steady-state turn [2]. The SSF is obtained by treating the vehicle as a rigid body and performing a sum of moments about the center of the right tire contact patch (point P in Figure 1.1).

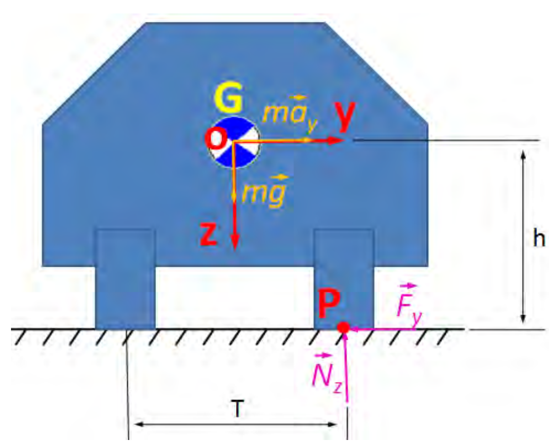

Figure 1.1: Free-body diagram of vehicle experiencing impending rollover [9].

Solving the moment equation and rearranging the terms provides the SSF value, expressed as:

$$SSF = \frac{a_y}{g} = \frac{T}{2h} \tag{1.1}$$

where a_y is the steady-state lateral acceleration, g is the gravitational acceleration, T is the average of the vehicle's front and rear track widths, and h is the height of the vehicle's center of gravity from the ground. Although the SSF and other static metrics provide useful information, their results are based on steady-state behavior and cannot fully characterize the roll stability of a vehicle during dynamic driving conditions, such as aggressive steering maneuvers. These methods are also empirical in nature, making them difficult to use for design and warning capabilities.

These concerns are addressed when utilizing dynamic model-based rollover metrics. Examples of these metrics include the Dynamic Stability Index (DSI) [3], the Time-To-Rollover (TTR) metric [4], the Load Transfer Ratio (LTR) [5], and the Stability Moment (SM) metric [6]. The first of these metrics, the DSI, utilizes the same rigid vehicle model as the SSF, but accounts for the inertia and angular acceleration of the vehicle as seen in Figure 1.2. Once again, the vehicle is assumed to be symmetrical, rigid, and traveling on a flat surface. The vehicle is also assumed to be on the threshold of rollover, resulting in negligible forces on the left tires. Performing a sum of moments about the center of the right tire contact patch (point P in Figure 1.2) and rearranging the terms yields the following equation:

$$DSI = \frac{T}{2h} = \frac{a_y}{g} - \frac{I_{xx}\,\alpha_x}{mgh} \tag{1.2}$$

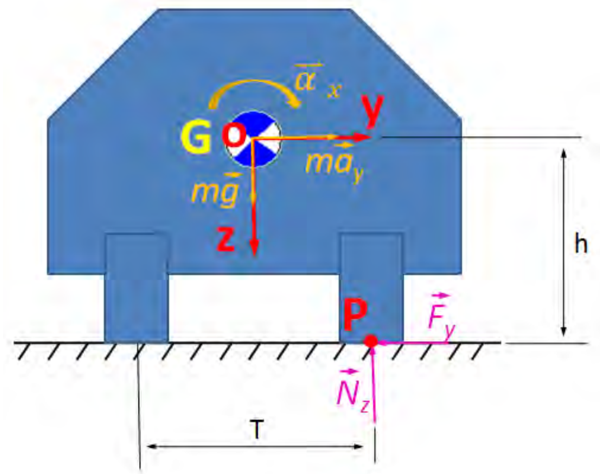

Figure 1.2: Free-body diagram experiencing impending rollover [9].

where a_y is the steady-state lateral acceleration, g is the gravitational acceleration, T is the average of the vehicle's front and rear track widths, h is the height of the vehicle's center of gravity, I_{xx} is the x-axis mass moment of inertia, α_x is the roll acceleration, and m is the mass of the vehicle.

Another dynamic metric that anticipates future rollover is the Time-To-Rollover (TTR) [4] which was originally proposed by Chen and Peng. Essentially, the TTR is defined as the time it will take for the sprung mass of the vehicle to reach a critical roll angle (wheel liftoff) with respect to the vehicle's unsprung mass over a predicted time interval. TTR calculates the vehicle's roll angle in the future and checks the value against a specified threshold. If the value is larger than the threshold, the time-to-rollover is established. This metric uses a 3-degree-of-freedom model and assumes that the steering angle remains constant throughout the predicted time interval. A flow chart of the TTR algorithm can be seen in Figure 1.3.

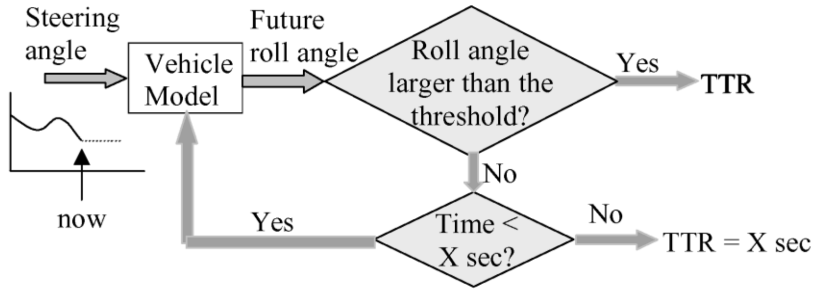

Figure 1.3: Flowchart of the Time-To-Rollover algorithm [4].

Finally, dynamic metrics can be derived by using vehicle-ground forces and moments. The Load Transfer Ratio (LTR) [5] and the Stability Moment (SM) [6] are two examples of such metrics. The LTR is defined as the ratio of the difference in normal forces of the right and left tires divided by the sum of the normal forces in the right and left tires. This metric, proposed by Ervin [5] at the University of Michigan Transportation Research Institute, can be written as the following equation:

$$LTR = \frac{F_{zR} - F_{zL}}{F_{zR} + F_{zL}} \tag{1.3}$$

where F_{zR} is the normal force acting on the right tire and F_{zL} is the normal force acting on the left tire. The LTR can only vary between -1 and 1, where a value of 1 represents wheel liftoff on the left side of the vehicle and a value of -1 represents wheel liftoff on the right side of the vehicle.

Similar to the LTR, the Stability Moment (SM) also utilizes vehicle-ground forces. This metric was proposed by Peters and Iagnemma [6] and can be viewed as an extension of the LTR. The SM is defined as the moment produced by the vehicle-ground contact forces about the tip-over axes of the vehicle. The tip-over axes are the lines connecting the contact points of the tires. The metric is then calculated as the ratio of the difference in the SMs of the right and left side divided by the sum of the SMs of the right and left side, resulting in the following equation:

$$R_{SM} = \frac{SM_L - SM_R}{SM_L + SM_R} \tag{1.4}$$

where SM_L is the Stability Moment on the left side of the vehicle and SM_R is the Stability Moment on the right side of the vehicle. Once again, the metric varies between values of -1 and 1 with the same implications. Metrics such as the LTR and SM rely on the knowledge of vehicle-ground contact forces. In practice, however, these forces are very difficult to measure. Sensors capable of obtaining this data are expensive and uncommon on typical passenger vehicles. These metrics also saturate at the onset of wheel liftoff, meaning they are unable to predict the severity of a potential rollover-inducing maneuver.

1.2 Zero-Moment Point

To address the limitations of the metrics presented above, previous work by the Intelligent Vehicles and Systems Research Group (IVSG) at Penn State [7-11] developed a dynamic rollover metric utilizing the concept of the Zero-Moment Point (ZMP). The zero-moment point is defined as the point on the ground where the summation of the tipping moments acting on an object, due to gravity and inertia forces, equals zero [12]. This concept was originally developed by Vukobratovic [13] in 1968 and has been applied to maintain the dynamic stability of bipedal robots. To remain in equilibrium, the location of the robot's ZMP must lie within its contact polygon; otherwise, the robot will overturn. This concept can be applied to a general object for further understanding. Figure 1.4(a) shows a mass resting on a tilt table.

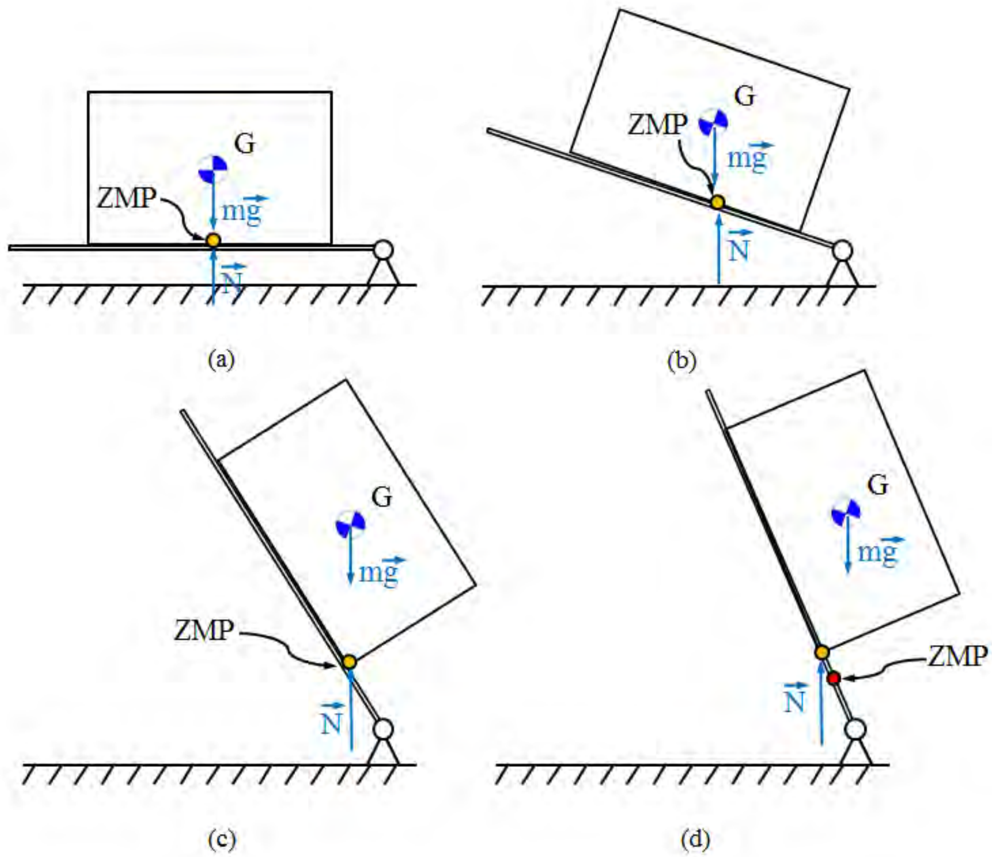

Figure 1.4: Free-body diagrams of mass on a tilt table [9].

The table is assumed to have enough friction that the mass does not slip. In Figure 1.4(a), the reaction force $\vec{N}$ lies directly below the object's center of mass. The point where this reaction acts is the ZMP. As the object is progressively inclined as seen in Figure 1.4(b), 1.4(c), and 1.4(d), the reaction force shifts to the right to balance the moment created by gravity and satisfy the definition of ZMP. Once the table is tilted to an angle that the ZMP is located outside the object's contact polygon as seen in Figure 1.4(d), the object is no longer stable and will overturn.

Applying the concept of the zero-moment point as a vehicle rollover metric presents several advantages. One advantage of the ZMP is that it explicitly accounts for terrain effects in its derivation. Another one of its more significant advantages is that calculation of the ZMP does not rely on knowledge of the vehicle-ground contact forces. By treating the vehicle as a kinematic chain, it is possible to calculate each body's net moment contribution to the zero-moment point. This calculation only requires measurement of the kinematic motion of all objects in the chain, information that is accessible through inertial measurement units and knowledge of the vehicle parameters. The formulation and application of the ZMP is discussed later in the paper.

1.3 Vehicle Preview Models

It is the goal of this research to explore vehicle path following and rollover prevention strategies with application towards autonomous vehicles. Ultimately, this research will help in optimizing a vehicle's road departure trajectory to prevent both collision and rollover. To achieve this, a vehicle preview model is developed that predicts both the vehicle's position and rollover propensity at a fixed time in the future. The ZMP metric is used in this preview model to predict the threat of rollover.

Nearly all driver models implement previewed information, or put another way, knowledge of what lies beyond the driver. Several preview control models have been developed that focus on vehicle path following, which predicts the vehicle's position at a fixed time or distance in the future. Two approaches to the problem of linear optimal control were found in the literature: predictive control theory and linear quadratic regulator (LQR) theory. Predictive control theory was used by MacAdam [14] in 1981 to develop an optimal preview controller for vehicle steering. This time-invariant controller uses a linear vehicle model and relies on the assumption that the steering input remains constant over the preview interval. Essentially, the controller minimizes the vehicle's lateral position error using a local performance index (cost function). By projecting the current states and inputs of the dynamic system over the preview interval, this model calculates an optimal control (steering input) that minimizes the error between the previewed input (the road) and the previewed output (the predicted vehicle path), as seen in Figure 1.5. Projection of the current vehicle states is done through the use of the system's state transition matrix [15].

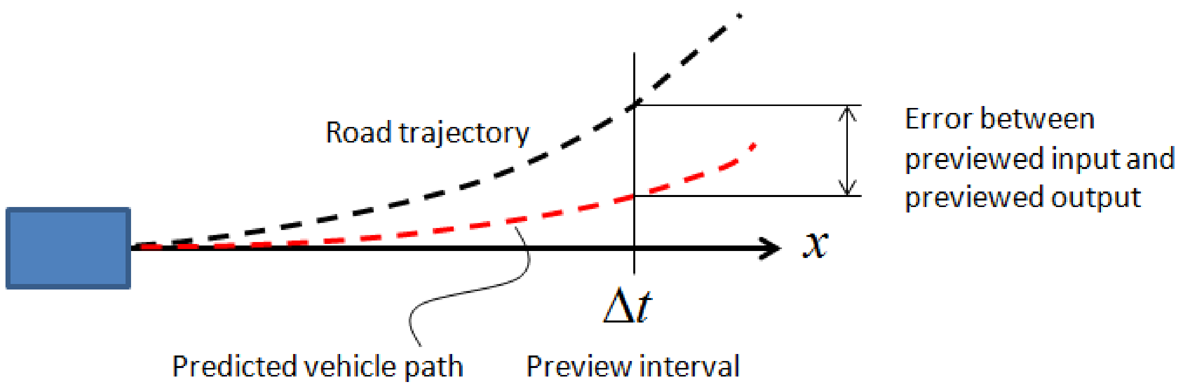

Figure 1.5: Error between road trajectory and predicted vehicle path over a specified preview interval.

Linear quadratic regulator (LQR) theory was used by Sharp and Valtetsiosis [16,17] in 2001 to develop another optimal preview controller. This controller used previewed road geometry to minimize a similar cost function regarding lateral path error with the addition of yaw path error and steering input. Use of the LQR theory assumed that the steering input could vary over an infinite horizon. In 2006, Cole and Pick [18] compared controllers using the two different theories and drew several conclusions. For predictive control theory, path-following errors are evaluated up to the preview horizon of the road path, while steering input is only calculated up to the control horizon. The control horizon must be less than or equal to the preview horizon for predictive control theory. For LQR theory, road path is previewed up to the preview horizon, but path-following errors are evaluated up to the control horizon rather than the preview horizon. The control horizon is independent of the preview horizon and can be set to any length. In the controller developed by Sharp and Valtetsiotis [16], the control horizon is set to infinity. While there are slight differences in the cost functions of the theories, both controllers approximate human behavior well and are identical when using preview and control horizons that are sufficiently long.

This research will make use of the MacAdam preview model in the path following problem. The Zero-Moment Point (ZMP) rollover metric will also be implemented to predict the vehicle's rollover propensity over the preview horizon. Further explanation and derivation of the MacAdam preview model and ZMP are discussed in subsequent sections of the report. This previewed information is then ultimately included in an overall output vector from the vehicle model. Determining reliable methods for path following and rollover prevention is an important step in optimizing a vehicle's trajectory to minimize rollover and road departure.

1.4 Outline of Remaining Chapters

The remainder of this thesis is organized as follows: Chapter 2 presents the derivations of the vehicle models used in this research. This includes 2- and 3-degree-of-freedom models with consideration of terrain influences and tire lag effects. Chapter 3 introduces the vehicle path following problem. The methodology of previewing the dynamic system is presented and then applied to the lateral position of the vehicle. The closed-loop MacAdam model is them derived and implemented to determine its effectiveness. Chapter 4 derives the concept of the zero-moment point as a vehicle rollover metric, which is then included as an output in the vehicle model. Previewed information about the ZMP is then explored and used to determine the minimum preview time needed to prevent rollover. Finally, Chapter 5 presents the conclusions made from this research and plans for future work.

1.5 References

[1] DOT, "2009 Traffic Safety Facts - Final Report," *U.S. Department of Transportation: National Highway Traffic Safety Board*, 2009.

[2] Transportation Research Board, *The National Highway Traffic and Safety Administration's Rating System for Rollover Resistance*. Washington, D.C.: National Academy Press, 2002.

[3] Dukkipati, R. V., J. Pang, M. S. Qatu, G. Sheng, and Z. Shuguang, *Road Vehicle Dynamics*, Warrendale, PA: Society of Automotive Engineers, Inc., 2008.

[4] B.-C. Chen and H. Peng, "Differential-braking-based rollover prevention for sport utility vehicle with human-in-the-loop," *Vehicle System Dynamics: International Journal of Vehicle Mechanics and Mobility*, vol. 36, no. 4-5, pp. 359–389, 2001.

[5] R. D. Ervin and Y. Guy, "The influence of weights and dimensions on the stability and control of heavy-duty trucks in Canada Volume I," The University of Michigan Transportation Research Institute, Ann Arbor, MI, Tech. Rep. UMTRI-86-35/I, July 1986.

[6] S. C. Peters and K. Iagnemma, "Stability measurement of high-speed vehicles," *Vehicle System Dynamics: International Journal of Vehicle Mechanics and Mobility*, vol. 47, no. 6, pp. 701–720, 2009.

[7] S. Lapapong and S. Brennan, “Terrain-aware rollover prediction for ground vehicles using the zero-moment point method,” in *Proc. American Control Conference*, Baltimore, MD, June 2010, pp. 1501–1507.

[8] S. Lapapong, A. A. Brown, and S. N. Brennan, “Experimental validation of terrain-aware rollover prediction for ground vehicles using the zero-moment point method,” in *10th International Symposium on Advanced Vehicle Control (AVEC2010)*, vol. 2, Longsborough, UK, Aug. 2010, pp. 1233–1237.

[9] S. Lapapong, “Vehicle rollover prediction for banked surfaces,” Ph.D. dissertation, The Pennsylvania State University, 2010.

[10] S. Lapapong and S. N. Brennan, “A novel comparative approach to evaluate vehicle rollover propensity,” in *Proc. of 2011 IAVSD*, Manchester, England, Aug 2011.

[11] S. Lapapong, A.A. Brown, K.S. Swanson, and S.N. Brennan, "Zero-moment point determination of worst case maneuvers leading the vehicle wheel lift." in *Vehicle System Dynamics: International Journal of Vehicle Mechanics and Mobility*, vol. 50, sup. 1, pp. 191-214, 2012.

[12] P. Sardain and G. Bessonnet, “Forces acting on a biped robot. center of pressure–zero moment point,” *IEEE Trans. Syst., Man, Cybern. A*, vol. 34, no. 5, pp. 630–637, Sept. 2004.

[13] M. Vukobratovic and D. Juricic, “Contribution to the synthesis of biped gait,” in *Proc. IFAC Symp. Technical and Biological Problem on Control*, Erevan, USSR, 1968.

[14] MacAdam, C. C. "Application of an Optimal Preview Control for Simulation of Closed-Loop Automobile Driving," *IEEE Transactions on Systems, Man, and Cybernetics*, SMC-11(6), pp. 393-399, 1981.

[15] F. Golnaraghi and B. Kuo, Automatic Control Systems, 9th ed. New York: John Wiley & Sons, Inc. 2010.

[16] Sharp, R. and V. Valtetsiotis, "Optimal preview car steering control," *Vehicle System Dynamics*, 35, pp. 101-117, 2001.

[17] Sharp, R. S. and H. Peng, "Vehicle Dynamics Applications of Optimal Control Theory," *Vehicle System Dynamics*, 49(7), pp. 1073-1111, 2011.

[18] Cole, D., A. Pick, and A. Odhams, "Predictive and linear quadratic methods for potential application to modelling driver steering control," *Vehicle System Dynamics*, 44(3), pp. 259-284, 2006.

Chapter 2 - Vehicle Dynamic Models

2.1 Two-Degree-of-Freedom Bicycle Model

A simple dynamic vehicle model commonly used is the two-degree-of-freedom (2DOF) bicycle model. This section will introduce the nomenclature and coordinate system used in vehicle models and derive the equations of motion of the bicycle model. These equations are then be used to develop a state-space representation of the vehicle.

The 2DOF bicycle model only considers the vehicle's lateral and yaw dynamics. The body-fixed coordinate system used to derive this model was developed by the Society of Automotive Engineers (SAE) [1] and is shown in Figure 2.1 (looking at the back of the vehicle). The nomenclature used in the derivation is listed in Table 2.1 and illustrated in Figure 2.2.

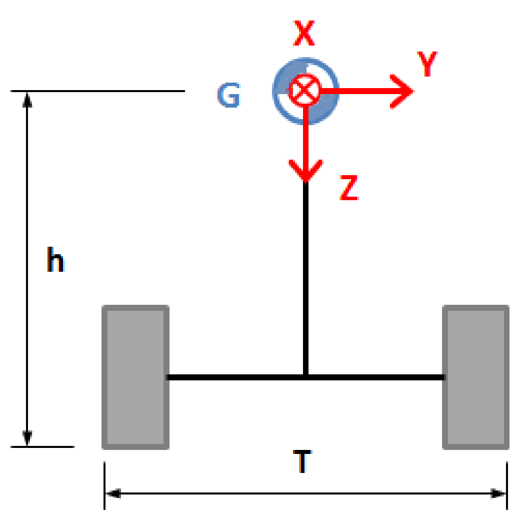

Figure 2.1: SAE Body-Fixed Vehicle Coordinate System.

Table 2.1: Bicycle model nomenclature.

Parameter	Definition
U	Longitudinal velocity at CG (body-fixed frame)
V	Lateral velocity at CG (body-fixed frame)
r	Yaw rate
m	Vehicle mass
I_{zz}	Mass moment of inertia about vehicle z-axis
a	Distance from CG to front axle along the x-axis
b	Distance from CG to rear axle along x-axis
L	Length of vehicle
T	Track width of vehicle
F_f	Front tire force
F_r	Rear tire force
$C_{\alpha f}$	Front cornering stiffness
$C_{\alpha r}$	Rear cornering stiffness
α_f	Front tire slip angle
α_r	Rear tire slip angle
δ_f	Front steering angle

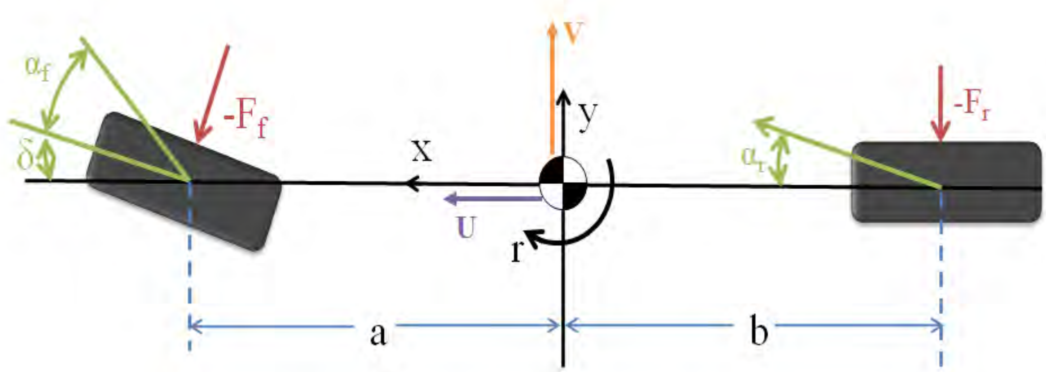

Figure 2.2: Free-body diagram of bicycle model in body-fixed coordinates.

The simplified bicycle model relies on several assumptions that are listed below:

- In the nature of a bicycle, the vehicle is assumed to be symmetrical along its longitudinal axis.
- No motion exists in the roll and pitch directions.
- The vehicle is steered by the front wheel.
- Longitudinal velocity, U, is assumed to be constant.
- Small angle approximation apply such that $\sin(\theta) \approx \theta$ and $\cos(\theta) \approx 1$.
- A linear tire model is applied such that $F = C_\alpha \alpha$. This statement says that the lateral force acting on the tire is linearly proportional to the tire side-slip angle.
- All components of the model are assumed to be rigid bodies.
- The tires are assumed to roll without slipping in the longitudinal direction.
- Aerodynamic effects are assumed to be negligible.

These assumptions allow the vehicle to be analyzed by the model shown in Figure 2.2. It should be noted that although this model is termed the bicycle model, it does not represent the dynamics of an actual bicycle.

Using the SAE body-fixed coordinate system described previously, the angular velocity and angular acceleration of the vehicle can be written as the following:

$$\vec{\omega} = r\hat{k} \tag{2.1}$$

$$\vec{\alpha} = \dot{r}\hat{k} \tag{2.2}$$

The linear velocity of the vehicle's center of gravity can be expressed as:

$$\vec{v}_o = U\hat{\imath} + V\hat{\jmath} \tag{2.3}$$

To apply Newton's equations, however, the accelerations of the vehicle must be written with respect to a global, Earth-fixed coordinate system. The Earth-fixed acceleration of a moving object can be written by the general equation

$$\vec{a} = \dot{\vec{v}}_{o,moving} + \vec{\omega} \times \vec{v}_{o,moving} \tag{2.4}$$

where $\vec{a}$ is the Earth-fixed acceleration of the object. Solving this equation yields the following for the total acceleration of the vehicle in Earth-fixed coordinates:

$$\vec{a} = \dot{U}\hat{\imath} + \dot{V}\hat{\jmath} + Ur\hat{\jmath} - Vr\hat{\imath} \tag{2.5}$$

$$\vec{a} = (-Vr)\hat{\imath} + (\dot{V} + Ur)\hat{\jmath} \tag{2.6}$$

where $\dot{U} = 0$ due to the constant velocity of the vehicle in the body-fixed longitudinal direction. Now the equations of motion for the vehicle can be written. The constant longitudinal velocity of the vehicle also means that the sum of forces in the longitudinal direction is equal to zero. Therefore, referring back to Figure 2.2, a sum of forces in the lateral direction and a sum of moments about the z-axis yield the equations of motion for the bicycle model.

$$\Sigma F_y = ma_y = m\big(\dot{V} + Ur\big) = F_f + F_r \tag{2.7}$$

$$\Sigma M_z = I_{zz}\dot{r} = aF_f - bF_r \tag{2.8}$$

Applying the assumption of the linear tire model, the front and rear tire forces can be expressed as $F_f = C_{\alpha f}\,\alpha_f$ and $F_r = C_{\alpha r}\,\alpha_r$ respectively. Substituting these forces into Equations 2.7 and 2.8 yields the following:

$$m(\dot{V} + Ur) = C_{\alpha f}\alpha_f + C_{\alpha r}\alpha_r \tag{2.9}$$

$$I_{zz}\dot{r} = aC_{\alpha f}\alpha_f - bC_{\alpha r}\alpha_r \tag{2.10}$$

The geometry of Figure 2.2 allows the tire slip angles to be written as functions of the velocities of each tire and the front steering angle in the form

$$\alpha_f = \tan^{-1}\left(\frac{v_{fy}}{v_{fx}}\right) - \delta_f = \left(\frac{v_{fy}}{v_{fx}}\right) - \delta_f = \frac{V + ar}{U} - \delta_f \tag{2.11}$$

$$\alpha_r = \tan^{-1}\left(\frac{v_{ry}}{v_{rx}}\right) = \left(\frac{v_{ry}}{v_{rx}}\right) = \frac{V - br}{U} \tag{2.12}$$

Small angle approximations assume that the inverse tangent function is approximately equal to the angle itself. Substituting Equations 2.11 and 2.12 into Equations 2.9 and 2.10 yields the final equations of motion for the bicycle model.

$$m(\dot{V} + Ur) = C_{\alpha f}\left(\frac{V + ar}{U} - \delta_f\right) + C_{\alpha r}\left(\frac{V - br}{U}\right) \tag{2.13}$$

$$I_{zz}\dot{r} = aC_{\alpha f}\left(\frac{V + ar}{U} - \delta_f\right) - bC_{\alpha r}\left(\frac{V - br}{U}\right) \tag{2.14}$$

Rearranging to solve for $\dot{V}$ and $\dot{r}$ yields the following:

$$\dot{V} = \left(\frac{C_{\alpha f} + C_{\alpha r}}{mU}\right)V + \left(\frac{aC_{\alpha f} - bC_{\alpha r}}{mU} - U\right)r - \left(\frac{C_{\alpha f}}{m}\right)\delta_f \tag{2.15}$$

$$\dot{r} = \left(\frac{aC_{\alpha f} - bC_{\alpha r}}{I_{zz}U}\right)V + \left(\frac{a^2C_{\alpha f} + b^2C_{\alpha r}}{I_{zz}U}\right)r - \left(\frac{aC_{\alpha f}}{I_{zz}}\right)\delta_f \tag{2.16}$$

Representing Equations 2.15 and 2.16 in matrix notation allows the equations of motion to be written as a state-space model with states of V and r. The state-space vehicle dynamic bicycle model is:

$$\begin{bmatrix}\dot{V}\\ \dot{r}\end{bmatrix}=\begin{bmatrix}\frac{C_{\alpha f}+C_{\alpha r}}{mU} & \frac{aC_{\alpha f}-bC_{\alpha r}}{mU}-U\\ \frac{aC_{\alpha f}-bC_{\alpha r}}{I_{zz}U} & \frac{a^2C_{\alpha f}+b^2C_{\alpha r}}{I_{zz}U}\end{bmatrix}\begin{bmatrix}V\\ r\end{bmatrix}+\begin{bmatrix}\frac{-C_{\alpha f}}{m}\\ \frac{-aC_{\alpha f}}{I_{zz}}\end{bmatrix}\delta_f \tag{2.17}$$

$$y=\begin{bmatrix}1 & 0\\ 0 & 1\end{bmatrix}\begin{bmatrix}V\\ r\end{bmatrix}+\begin{bmatrix}0\\ 0\end{bmatrix}\delta_f$$

2.2 Three-Degree-of-Freedom Roll Model

Although the bicycle model is useful for understanding the lateral and yaw accelerations of the vehicle, it does not provide any information about the vehicle's roll characteristics. This section introduces a three-degree-of-freedom roll model mathematically consistent with the vehicle model developed by Mammar [2] in 1999, with the exception of the coordinate system location. This model is considered an extension of the bicycle model to understand the effects of the vehicle's suspension by including roll dynamics.

The nomenclature and coordinate system used to derive this roll model are listed in Table 2.2 and illustrated in Figure 2.3. The equations of motions will be derived and written in mass-damper-spring from. These equations will then be used to develop a state-space representation of the vehicle.

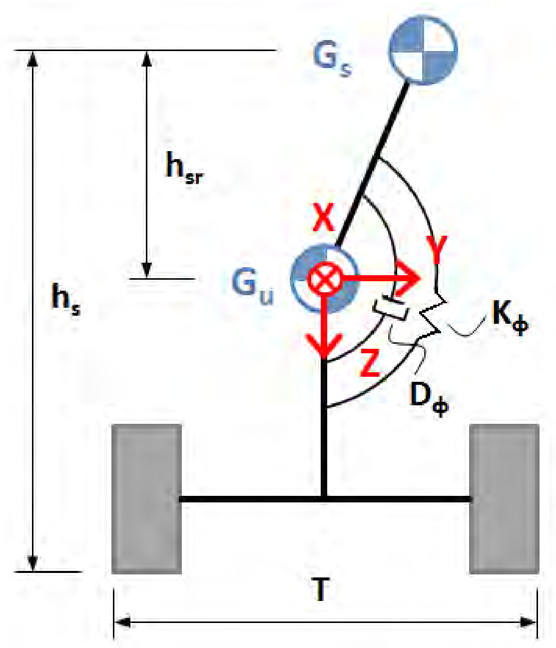

Figure 2.3: Free-body diagram of roll model in body-fixed coordinates.

Table 2.2: Roll model nomenclature.

Parameter	Definition
U	Longitudinal velocity at CG (body-fixed frame)
V	Lateral velocity at CG (body-fixed frame)
ϕ	Roll angle of sprung mass
p	Roll rate of sprung mass
r	Yaw rate
m	Total vehicle mass
m_u	Unsprung vehicle mass
m_s	Sprung vehicle mass
I_{xx}	Mass moment of inertia about vehicle x-axis
I_{zz}	Mass moment of inertia about vehicle z-axis
I_{xz}	Product mass moment of inertia
a	Distance from CG to front axle along the x-axis
b	Distance from CG to rear axle along x-axis
L	Length of vehicle
T	Track width of vehicle
h_r	Height of roll center
h_s	Height of sprung mass CG
h_{sr}	Height of sprung mass CG from roll center
F_f	Front tire force
F_r	Rear tire force
$C_{\alpha f}$	Front cornering stiffness
$C_{\alpha r}$	Rear cornering stiffness
α_f	Front tire slip angle
α_r	Rear tire slip angle
δ_f	Front steering angle
K_ϕ	Roll stiffness
D_ϕ	Roll damping constant
g	Gravitational acceleration

Similar to the bicycle model, the three-degree-of-freedom roll model relies on the following assumptions to aid in its derivation:

- The vehicle is assumed to be symmetrical along its longitudinal axis ($I_{xy\,=\,0}$).
- No motion exists in the pitch direction.
- The vehicle is steered by the front wheel.
- Longitudinal velocity, U, is assumed to be constant.
- Small angle approximation apply such that $\sin(\theta) \approx \theta$ and $\cos(\theta) \approx 1$.
- A linear tire model is applied such that $F = C_\alpha\, \alpha$. This statement says that the lateral force acting on the tire is linearly proportional to the tire side-slip angle.
- All components of the model are assumed to be rigid bodies.
- The tires are assumed to roll without slipping in the longitudinal direction.
- Aerodynamic effects are assumed to be negligible.
- The torsional spring and torsional damper acting at the roll center are linear.
- The roll center is fixed with respect to the vehicle's body
- The unsprung mass only rotates in the yaw direction.

Referring to Figure 2.3, the roll model can be described as dividing the vehicle mass into a sprung mass (G_s) and an unsprung mass (G_u). The sprung mass represents the mass of the vehicle that sits on top of the suspension while the unsprung mass represents the mass of the vehicle that is located under, and thus is unaffected by, the vehicle's suspension. These two masses are connected at a joint called the roll center, which is defined as the virtual point about which the suspension rolls with respect to the unsprung mass. A torsional spring and torisonal damper have been included at the roll center to simulate the vehicle's suspension dynamics. As indicated in the model assumptions, the roll center only allows rotation about the vehicle's longitudinal axis. For this derivation, the vehicle coordinate system has been attached to the unsprung mass.

Considering the coordinate system shown in Figure 2.3, the angular velocity of the unsprung mass can be written as:

$$\vec{\omega}_u = r\hat{k} \tag{2.18}$$

while the angular velocity of the sprung mass can be written as:

$$\vec{\omega}_s = \dot{\phi}\hat{\imath} + r\hat{k} \tag{2.19}$$

Similarly, the linear velocity of the unsprung mass can written as:

$$\vec{v}_u = U\hat{\imath} + V\hat{\jmath} \tag{2.20}$$

while the linear velocity of the sprung mass can be written as:

$$\vec{v}_s = U\hat{\imath} + (V + h_{sr}\dot{\phi})\hat{\jmath} \tag{2.21}$$

Equation 2.21 was derived by utilizing relative velocity and assuming a small roll angle. To determine the accelerations of the sprung and unsprung masses, the velocities must be converted to a global, Earth-fixed coordinate system. This allows Newton's equations to be used to describe the system. The Earth-fixed acceleration of a moving object can be written by the general equation

$$\vec{a} = \dot{\vec{v}}_{o,moving} + \vec{\omega} \times \vec{v}_{o,moving} \tag{2.22}$$

where $\vec{a}$ is the Earth-fixed acceleration of the object. Solving this equation for the unsprung mass and assuming the roll center is coincident with the unsprung mass's CG yields the following equation:

$$\vec{a}_u = \dot{U}\hat{\imath} + \dot{V}\hat{\jmath} + Ur\hat{\jmath} - Vr\hat{\imath} \tag{2.23}$$

$$\vec{a}_u = (-Vr)\hat{\imath} + (\dot{V} + Ur)\hat{\jmath} \tag{2.24}$$

where $\dot{U} = 0$ due to the constant velocity of the vehicle in the body-fixed longitudinal direction. The acceleration of the sprung mass can be calculated as

$$\vec{a}_s = \dot{U}\hat{\imath} + \left(\dot{V} + h_{sr}\ddot{\phi}\right)\hat{\jmath} - r\left(V + h_{sr}\dot{\phi}\right)\hat{\imath} + Ur\hat{\jmath} + V\dot{\phi}\hat{k} \tag{2.25}$$

$$\vec{a}_s = -r\left(V + h_{sr}\dot{\phi}\right)\hat{\imath} + \left(\dot{V} + Ur + h_{sr}\ddot{\phi}\right)\hat{\jmath} + V\dot{\phi}\hat{k} \tag{2.26}$$

Now the equations of motion for the vehicle can be written. The inclusion of roll dynamics adds another equation of motion, obtained by performing a sum of moments about the vehicle's x-axis. Therefore, the three equations are obtained through a sum of forces in the lateral direction, a sum of moments about the vehicle's z-axis, and a sum of moments about the vehicles x-axis. Summing the forces in the lateral direction yields the following equation:

$$\Sigma F_y = m_u a_{yu} + m_s a_{ys} = F_f + F_r \tag{2.27}$$

$$m\left(\dot{V} + Ur\right) + m_s h_{sr}\ddot{\phi} = F_f + F_r \tag{2.28}$$

The next equation of motion is obtained by summing the moments about the roll center in the x-direction. Assuming the vehicle's roll center is close to the ground, the equation can be written as

$$\Sigma M_{x,RC} = I_{xx}\ddot{\phi} - I_{xz}\dot{r} + m_s\left(\left(-h_{sr}\hat{k}\right) \times \vec{a}_s\right) \cdot \hat{\imath} \tag{2.29}$$

$$I_{xx}\ddot{\phi} - I_{xz}\dot{r} + m_s h_{sr}\left(\dot{V} + Ur + h_{sr}\ddot{\phi}\right) = -D_\phi\dot{\phi} + (m_s h_{sr} g - K_\phi)\phi \tag{2.30}$$

The last equation of motion is developed by summing the moments in the yaw direction about the sprung mass CG to produce the following:

$$\Sigma M_{z,s} = I_{zz}\dot{r} - I_{xz}\ddot{\phi} + m_s\left(\left(-h_{sr}\hat{k}\right) \times \vec{a}_s\right) \cdot \hat{k} = aF_f - bF_r \tag{2.31}$$

$$I_{zz}\dot{r} - I_{xz}\ddot{\phi} = aF_f - bF_r \tag{2.32}$$

Equations 2.28, 2.30, and 2.32 represent the three equations of motion for the roll model. These can be organized in the standard mass-damper-spring (MDK) form of

$$M\ddot{q} + D\dot{q} + Kq = Fu_f \tag{2.33}$$

where

$$q = \begin{bmatrix} y \\ \psi \\ \phi \end{bmatrix} \tag{2.34}$$

defines the states of the MDK equation. These are the three-degrees-of-freedom of the roll model; y is the lateral position, ψ is the yaw angle, and ϕ is the roll angle. By rearranging the three equations of motion, the mass, damper, and spring matrices are defined as

$$M = \begin{bmatrix} m & 0 & m_s h_{sr} \\ m_s h_{sr} & -I_{xz} & I_{xx} + m_s h_{sr}^2 \\ 0 & I_{zz} & -I_{xz} \end{bmatrix} \tag{2.35}$$

$$D = \begin{bmatrix} 0 & mU & 0 \\ 0 & m_s h_{sr} U & D_\phi \\ 0 & 0 & 0 \end{bmatrix} \tag{2.36}$$

$$K = \begin{bmatrix} 0 & 0 & 0 \\ 0 & 0 & K_\phi - m_s h_{sr} g \\ 0 & 0 & 0 \end{bmatrix} \tag{2.37}$$

The input to the model is defined as the front and rear tire forces in the lateral direction such that

$$u = \begin{bmatrix} F_f \\ F_r \end{bmatrix} \tag{2.38}$$

and the force matrix is defined as

$$F = \begin{bmatrix} 1 & 1 \\ a & -b \\ 0 & 0 \end{bmatrix} \tag{2.39}$$

The equations of motion for the roll model can also be represented in general state-space form, which allows easier numerical simulation of the system. The state-space form can be derived from the MDK form by first breaking down the lateral forces acting on the system by applying the assumption of the linear tire model such that $F_f = C_{\alpha f} \alpha_f$ and $F_r = C_{\alpha r} \alpha_r$. Referring back to Figure 2.2, the tire slip angles can be written as functions of the velocities of each tire and the front steering angle.

$$\alpha_f = \tan^{-1}\left(\frac{v_{fy}}{v_{fx}}\right) - \delta_f = \left(\frac{v_{fy}}{v_{fx}}\right) - \delta_f = \frac{V + ar}{U} - \delta_f \tag{2.40}$$

$$\alpha_r = \tan^{-1}\left(\frac{v_{ry}}{v_{rx}}\right) = \left(\frac{v_{ry}}{v_{rx}}\right) = \frac{V - br}{U} \tag{2.41}$$

Substituting Equations 2.11 and 2.12 into the lateral forces produces the three equations of motion after some rearrangement in the following form:

$$m\dot{V} + m_s h_{sr}\ddot{\phi} + \left(mU + \frac{bC_{\alpha r} - aC_{\alpha f}}{U}\right)r + \left(\frac{-C_{\alpha f} - C_{\alpha r}}{U}\right)V = -C_{\alpha f}\delta_f \qquad (2.42)$$

$$\begin{gathered}(I_{xx} + m_s h_{sr}^2)\ddot{\phi} + m_s h_{sr}\dot{V} - I_{xz}\dot{r} + m_s h_{sr}Ur + D_\phi\dot{\phi} \\ - \left(m_s h_{sr} g - K_\phi\right)\phi = 0\end{gathered} \qquad (2.43)$$

$$I_{zz}\dot{r} - I_{xz}\ddot{\phi} + \left(\frac{-a^2C_{\alpha f} - b^2C_{\alpha r}}{U}\right)r + \left(\frac{bC_{\alpha r} - aC_{\alpha f}}{U}\right)V = -aC_{\alpha f}\delta_f \qquad (2.44)$$

By introducing a fourth equation,

$$\dot{\phi} = \dot{\phi} \qquad (2.45)$$

an intermediate MDK model can be introduced in the form

$$M_{int}\dot{x} + N_{int}x = F_{int}\delta_f \qquad (2.46)$$

The state vector of this intermediate model, and ultimately the state-space model, is then defined as

$$x = \begin{bmatrix} V \\ r \\ \dot{\phi} \\ \phi \end{bmatrix} \qquad (2.47)$$

Writing the equations of motion in the form of Equation 2.46 results in the following matrices:

$$M_{int} = \begin{bmatrix} m & 0 & m_s h_{sr} & 0 \\ m_s h_{sr} & -I_{xz} & I_{xx} + m_s h_{sr}^2 & 0 \\ 0 & I_{zz} & -I_{xz} & 0 \\ 0 & 0 & 0 & 1 \end{bmatrix} \qquad (2.48)$$

$$N_{int} = \begin{bmatrix} \frac{-C_{\alpha f} - C_{\alpha r}}{U} & mU + \frac{bC_{\alpha r} - aC_{\alpha f}}{U} & 0 & 0 \\ 0 & m_s h_{sr} U & D_\phi & K_\phi - m_s h_{sr} g \\ \frac{bC_{\alpha r} - aC_{\alpha f}}{U} & \frac{-a^2 C_{\alpha f} - b^2 C_{\alpha r}}{U} & 0 & 0 \\ 0 & 0 & -1 & 0 \end{bmatrix} \tag{2.49}$$

The input to the intermediate model is the front steering angle, δ_f, with a force matrix of

$$F_{int} = \begin{bmatrix} -C_{\alpha f} \\ 0 \\ -aC_{\alpha f} \\ 0 \end{bmatrix} \tag{2.50}$$

The general state-space form of

$$\dot{x} = Ax + Bu \tag{2.51}$$

with a state vector described in Equation 2.47, can easily be obtained from this intermediate form through the relationship

$$A = -M_{int}^{-1} N_{int} \tag{2.52}$$

$$B = M_{int}^{-1} F_{int} \tag{2.53}$$

2.3 Bicycle Model with Road Bank Angle Input

In many cases, the road profile is not perfectly level in the lateral direction. This is also the case just outside the road boundaries, as the terrain typically slopes down as it moves away from the road. Therefore, it is necessary to take the road bank angle into consideration for these driving situations. The terrain angle, ϕ_t as seen in Figure 2.4, will now be considered when developing the equations of motion.

For the two-degree-of-freedom bicycle model with small angle approximations, the terrain angle affects the equations of motion in the following manner:

$$\Sigma F_y = F_f + F_r + mg\sin\phi_t = F_f + F_r + mg\phi_t \tag{2.54}$$

$$\Sigma M_z = I_{zz}\dot{r} = aF_f - bF_r \tag{2.55}$$

Only the sum of forces in the lateral direction is affected by the inclusion of terrain angle; it has no contribution towards the sum of moments about the vehicle's z-axis.

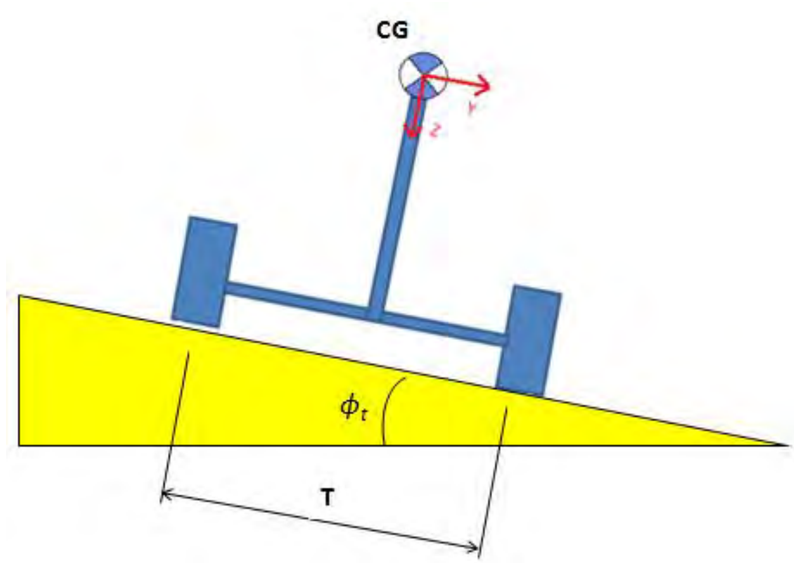

Figure 2.4: Rigid vehicle model on banked slope.

To maintain a linear system, the terrain angle is treated as a linear input to the system dynamics. The equations of motion with bank angle input result in the following state-space representation of the bicycle model:

$$\begin{bmatrix} \dot{V} \\ \dot{r} \end{bmatrix} = \begin{bmatrix} \dfrac{C_{\alpha f} + C_{\alpha r}}{mU} & \dfrac{aC_{\alpha f} - bC_{\alpha r}}{mU} - U \\ \dfrac{aC_{\alpha f} - bC_{\alpha r}}{I_{zz}U} & \dfrac{a^2 C_{\alpha f} + b^2 C_{\alpha r}}{I_{zz}U} \end{bmatrix} \begin{bmatrix} V \\ r \end{bmatrix} + \begin{bmatrix} \dfrac{-C_{\alpha f}}{m} & g \\ \dfrac{-aC_{\alpha f}}{m} & 0 \end{bmatrix} \begin{bmatrix} \delta_f \\ \phi_t \end{bmatrix} \tag{2.56}$$

$$y = \begin{bmatrix} 1 & 0 \\ 0 & 1 \end{bmatrix} \begin{bmatrix} V \\ r \end{bmatrix} + \begin{bmatrix} 0 & 0 \\ 0 & 0 \end{bmatrix} \begin{bmatrix} \delta_f \\ \phi_t \end{bmatrix}$$

The terrain bank angle is typically defined in units of degrees or as a percent superelevation. When defined as a percent superelevation, this research uses the following equation:

$$\%\, superelevation = 100 * \tan\left(\frac{rise}{run}\right) \tag{2.57}$$

2.4 Roll Model with Road Bank Angle Input

Similar to the bicycle model, the equations of motion for the three-degree-of-freedom roll model are also affected by the inclusion of terrain angle, ϕ_t. A diagram of the roll model on a banked slope can be seen in Figure 2.5.

The terrain angle affects the equations of motion in the following manner:

$$\Sigma F_y = F_f + F_r + mg\sin\phi_t = F_f + F_r + mg\phi_t \tag{2.58}$$

$$\Sigma M_x = -D_\phi - K_\phi \phi + m_s h_{sr} g(\phi + \phi_t) \tag{2.59}$$

$$\Sigma M_z = I_{zz}\dot{r} = aF_f - bF_r \tag{2.60}$$

Once again, the terrain angle is assumed to not affect the sum of moments about the vehicle's z-axis and small angles approximations apply. These equations also assume a positive roll angle is measured clockwise from the roll center, as shown in Figure 2.5.

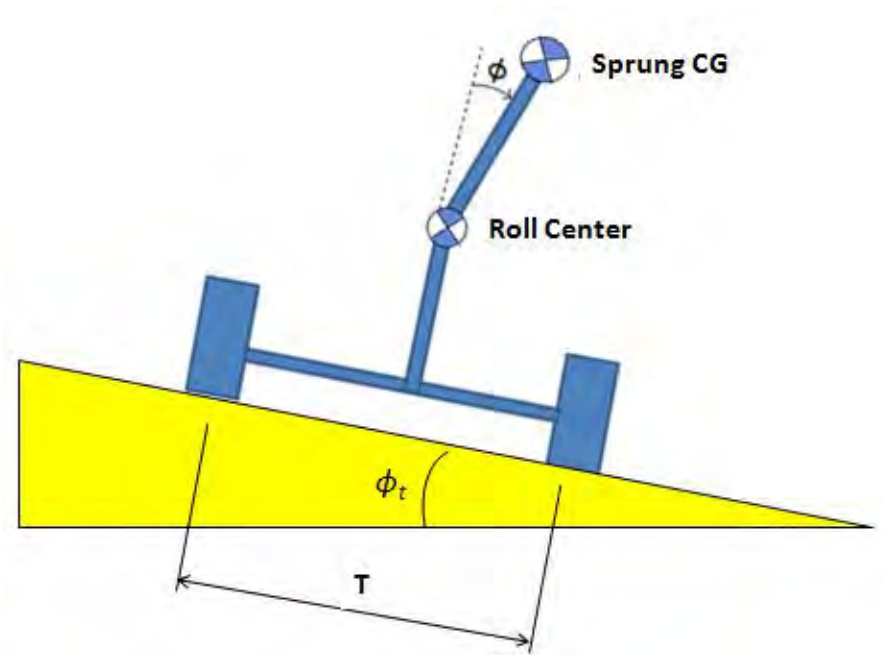

Figure 2.5: Roll model on a banked surface.

The terrain angle is treated as a linear input to the system dynamics, which can be written in the form

$$M_{int}\dot{x} + N_{int}x = F_{int}\begin{bmatrix}\delta_f \\ \phi_t\end{bmatrix} \tag{2.61}$$

where x is the state vector expressed in Equation 2.47. The matrices M_{int} and N_{int} are identical to those derived for the roll model without terrain angle and are expressed in Equations 2.48 and 2.49 respectively. The new F_{int} matrix includes the effects of the terrain angle and is written as

$$F_{int} = \begin{bmatrix} -C_{\alpha f} & mg \\ 0 & m_s h_{sr} g \\ -aC_{\alpha f} & 0 \\ 0 & 0 \end{bmatrix} \tag{2.62}$$

The general state-space form of

$$\dot{x} = Ax + Bu \tag{2.63}$$

with a state vector described in Equation 2.47, can easily be obtained from this form through the relationship

$$A = -M_{int}^{-1}N_{int} \tag{2.64}$$

$$B = M_{int}^{-1}F_{int} \tag{2.65}$$

2.5 Bicycle Model with Tire Lag Dynamics

An assumption of the models above was that the tires respond to and generate lateral force instantly from changes in steering input. In realistic driving situations, however, this is not true; due to deformation of the tire sidewall, there is a lag between the steering input and the force generated by the tires. Tire lag can affect the roll behavior of a vehicle and is important to consider in this work.

Tire lag is most commonly modeled as a first-order differential equation [3] in the form

$$\dot{F}_f = \frac{U}{\sigma}(F_{ss} - F_f) \tag{2.66}$$

$$\dot{F}_r = \frac{U}{\sigma}(F_{ss} - F_r) \tag{2.67}$$

where F_f and F_r are the front and rear tire forces, respectively, F_{ss} is the steady-state tire force, and σ is the tire relaxation length. As previously defined, the steady-state tire force is written as

$$F_{ss} = C_\alpha \alpha \tag{2.68}$$

where

$$\alpha_f = \frac{V + ar}{U} - \delta_f \tag{2.69}$$

$$\alpha_r = \frac{V - br}{U} \tag{2.70}$$

Substituting Equations 2.68, 2.69, and 2.70 allows the equations for the front and rear tire forces to be written in the form

$$\dot{F}_f = \frac{U}{\sigma}\left[C_{\alpha f}\left(\frac{V + ar}{U} - \delta_f\right) - F_f\right] \tag{2.71}$$

$$\dot{F}_r = \frac{U}{\sigma}\left[C_{\alpha r}\left(\frac{V - br}{U}\right) - F_r\right] \tag{2.72}$$

Inclusion of tire lag dynamics is done by adding the front and rear tire forces as states in the vehicle model. Using Equations 2.7 and 2.8, with the addition of Equations 2.71 and 2.72, results in an augmented state-space model in the following form:

$$\begin{bmatrix} \dot{V} \\ \dot{r} \\ \dot{F}_f \\ \dot{F}_r \end{bmatrix} = \begin{bmatrix} 0 & -U & \frac{1}{m} & \frac{1}{m} \\ 0 & 0 & \frac{a}{I_{zz}} & \frac{-b}{I_{zz}} \\ \frac{C_{\alpha f}}{\sigma} & \frac{C_{\alpha f} a}{\sigma} & \frac{-U}{\sigma} & 0 \\ \frac{C_{\alpha r}}{\sigma} & \frac{-C_{\alpha r} b}{\sigma} & 0 & \frac{-U}{\sigma} \end{bmatrix} \begin{bmatrix} V \\ r \\ F_f \\ F_r \end{bmatrix} + \begin{bmatrix} 0 \\ 0 \\ \frac{-C_{\alpha f} U}{\sigma} \\ 0 \end{bmatrix} \delta_f \tag{2.73}$$

When bank angle input is also considered, the model given by Equation 2.73 is slightly modified as

$$\begin{bmatrix} \dot{V} \\ \dot{r} \\ \dot{F}_f \\ \dot{F}_r \end{bmatrix} = \begin{bmatrix} 0 & -U & \frac{1}{m} & \frac{1}{m} \\ 0 & 0 & \frac{a}{I_{zz}} & \frac{-b}{I_{zz}} \\ \frac{C_{\alpha f}}{\sigma} & \frac{C_{\alpha f} a}{\sigma} & \frac{-U}{\sigma} & 0 \\ \frac{C_{\alpha r}}{\sigma} & \frac{-C_{\alpha r} b}{\sigma} & 0 & \frac{-U}{\sigma} \end{bmatrix} \begin{bmatrix} V \\ r \\ F_f \\ F_r \end{bmatrix} + \begin{bmatrix} 0 & g \\ 0 & 0 \\ \frac{-C_{\alpha f} U}{\sigma} & 0 \\ 0 & 0 \end{bmatrix} \begin{bmatrix} \delta_f \\ \phi_t \end{bmatrix} \tag{2.74}$$

2.6 Roll Model with Tire Lag Dynamics

Similar to the bicycle model, the tire lag effects of Equations 2.71 and 2.72 can be included in the vehicle roll model. Once again, the front and rear tire forces are added as states in the model. Using Equations 2.28, 2.30, 2.32, and 2.45, with the addition of Equations 2.71 and 2.72, the M_{int}, N_{int}, and F_{int} matrices of

$$M_{int}\dot{x} + N_{int}x = F_{int}\delta_f \tag{2.75}$$

can be modified in the following form:

$$M_{int} = \begin{bmatrix} m & 0 & m_s h_{sr} & 0 & 0 & 0 \\ m_s h_{sr} & -I_{xz} & I_{xx} + m_s h_{sr}^2 & 0 & 0 & 0 \\ 0 & I_{zz} & -I_{xz} & 0 & 0 & 0 \\ 0 & 0 & 0 & 1 & 0 & 0 \\ 0 & 0 & 0 & 0 & 1 & 0 \\ 0 & 0 & 0 & 0 & 0 & 1 \end{bmatrix} \tag{2.76}$$

$$N_{int} = \begin{bmatrix} 0 & mU & 0 & 0 & -1 & -1 \\ 0 & m_s h_{sr} U & D_\phi & K_\phi - m_s h_{sr} g & 0 & 0 \\ 0 & 0 & 0 & 0 & -a & b \\ 0 & 0 & -1 & 0 & 0 & 0 \\ \frac{-C_{\alpha f}}{\sigma} & \frac{-C_{\alpha f} a}{\sigma} & 0 & 0 & \frac{U}{\sigma} & 0 \\ \frac{-C_{\alpha r}}{\sigma} & \frac{C_{\alpha r} b}{\sigma} & 0 & 0 & 0 & \frac{U}{\sigma} \end{bmatrix} \tag{2.77}$$

$$F_{int} = \begin{bmatrix} 0 \\ 0 \\ 0 \\ 0 \\ \frac{-C_{\alpha f} U}{\sigma} \\ 0 \end{bmatrix} \tag{2.78}$$

where the state vector, x, of this intermediate model is given as

$$x = \begin{bmatrix} V \\ r \\ \dot{\phi} \\ \phi \\ F_f \\ F_r \end{bmatrix} \tag{2.79}$$

As discussed in Section 2.2, the general state-space form of

$$\dot{x} = Ax + Bu \tag{2.80}$$

can easily be obtained from this intermediate form through the relationship

$$A = -M_{int}^{-1} N_{int} \tag{2.81}$$

$$B = M_{int}^{-1} F_{int} \tag{2.82}$$

When bank angle input is also considered as a second input, the intermediate F_{int} matrix is written as

$$F_{int} = \begin{bmatrix} 0 & mg \\ 0 & m_s h_{sr} g \\ 0 & 0 \\ 0 & 0 \\ \dfrac{-C_{\alpha f} U}{\sigma} & 0 \\ 0 & 0 \end{bmatrix} \tag{2.83}$$

2.7 References

[1] “Surface Vehicle Recommended Practice,” Society of Automotive Engineers J670e, July 1976.

[2] S. Mammar, V. B. Baghdassarian, and L. Nouveliere, “Speed scheduled lateral vehicle control,” in *1999 International Conference on Intelligent Transportation Systems*, 1999, pp. 80–85.

[3] D. Karnopp, *Vehicle Stability*. 2004, New York: Marcel Dekker, Inc.

Chapter 3 - Vehicle Path Following

This chapter focuses on developing and implementing a vehicle path following preview model that is representative of a driver. The model presented in this chapter utilizes the work of MacAdam [1] in 1981 which predicts the vehicle's lateral position in the future and uses the information to develop a closed-loop steering controller. MacAdam's preview model uses the linear bicycle model and relies on the assumption of a constant steering input over the preview interval.

First, the methodology of calculating a fixed point preview of the vehicle's lateral position is discussed. This previewed information is then used to develop and check the validity of the MacAdam controller.

3.1 Fixed Point Preview

Predicting the states of a dynamic system in the future is necessary to develop preview controllers. Previewed information can be obtained by extending the current states and inputs of the system over a specified preview interval. Considering the following linear system,

$$\begin{aligned} \dot{x} &= Ax(t) + Bu(t) \\ y &= Cx(t) + Du(t) \end{aligned} \tag{3.1}$$

the general solution is given by

$$x(t+T) = \Phi(t+T,t)x(t) + \int_{t}^{t+T} \Phi(t+T,\tau)\, B(\tau)u(\tau)d\tau \tag{3.2}$$

where T is the preview time and Φ is the system's state transition matrix [2]. The state transition matrix is determined by the Peano-Baker series, which for a linear time-invariant system, reduces to the matrix exponential in the form

$$\Phi(t+T,t)=\sum_{k=0}^{\infty}\frac{A^k(T-t)^k}{k!}=e^{A(T-t)} \tag{3.3}$$

This solution given by Equation 3.2 allows the calculation of the state vector at time $t+T$ using the current state vector and the input during the preview time. To utilize this solution, several approximations of the state transition matrix exist. Euler, bilinear (Tustin), and numerical approximations of the state transition matrix were considered. Euler approximation results in the following:

$$\Phi(t+T,t)\approx I+TA \tag{3.4}$$

where I is the identity matrix. The bilinear approximation, also known as the Tustin transformation, provides greater accuracy and is given by

$$\Phi(t+T,t)\approx\frac{I+0.5TA}{I-0.5TA} \tag{3.5}$$

Numerical approximation of the state transition matrix is achieved by calculating the matrix exponential within MATLAB. This is considered an approximation because embedded function code within MATLAB does not calculate the matrix exponential to an exact solution.

The general solution given by Equation 3.2 can be applied to the vehicle path following problem. For this application, the desired output of the system is the previewed lateral position of the vehicle. When calculating the lateral position of the vehicle, the two-degree-of-freedom bicycle model and the three-degree-of-freedom roll model provide identical solutions. Therefore, only the simpler bicycle model is presented in this section. There were also negligible differences in lateral position when including tire lag effects; therefore, tire lag is not considered in this section.

To calculate the lateral position of the vehicle, the bicycle model is modified to include lateral position and yaw angle as states in the form

$$x = \begin{bmatrix} y \\ V \\ r \\ \psi \end{bmatrix} \tag{3.6}$$

The A and B matrices of the state space model then become

$$A = \begin{bmatrix} 0 & 1 & 0 & U \\ 0 & \dfrac{C_{\alpha f} + C_{\alpha r}}{mU} & \dfrac{aC_{\alpha f} - bC_{\alpha r}}{mU} - U & 0 \\ 0 & \dfrac{aC_{\alpha f} - bC_{\alpha r}}{I_{zz}U} & \dfrac{a^2C_{\alpha f} + b^2C_{\alpha r}}{I_{zz}U} & 0 \\ 0 & 0 & 1 & 0 \end{bmatrix} \tag{3.7}$$

$$B = \begin{bmatrix} 0 \\ \dfrac{-C_{\alpha f}}{m} \\ \dfrac{-aC_{\alpha f}}{I_{zz}} \\ 0 \end{bmatrix} \tag{3.8}$$

The previewed lateral position of the vehicle is then obtained by selecting the appropriate C and D output matrices in the state-space model. Recognizing that the A and B matrices are time invariant and utilizing the assumption that the steering input remains constant over the preview interval, the general solution of Equation 3.2 for the previewed state vector can be written as the following:

$$x(t+T) = \Phi(t+T,t)x(t) + Bu\int_{t}^{t+T}\Phi(t+T,\tau)\,d\tau \tag{3.9}$$

Equation 3.9 can also be rewritten in the form of an infinite series resulting in the following:

$$x(t+T) = \Phi(t+T,t)x(t) + \Psi TBu \tag{3.10}$$

where u is the steering input and

$$\Psi = I + \sum_{k=1}^{\infty}\frac{(TA)^k}{(k+1)!} \tag{3.11}$$

Using Equation 3.10 and the various state transition matrix approximations discussed previously results in the previewed state vector. Therefore, the previewed lateral position is obtained by simply pulling out the lateral position from the previewed state vector as an output of the system. It should be noted that Equation 3.11 does not quickly converge when elements of the A matrix are large. An alternate method of calculating the previewed input term for these situations is presented in Chapter 4.

To test the validity of the previewed lateral position calculation, MATLAB simulations were performed for a sinusoidal lane change maneuver steering input of amplitude 0.05 rad and frequency of 2 rad/s. The longitudinal velocity of 13.5 m/s (30 mph) is assumed to remain constant throughout the maneuver. This results in a standard 3.5 m lane change over 3 seconds. Vehicle parameters for a laden 1989 GMC 2500 pick-up truck were used in the simulations and are listed in Table 3.1.

The previewed lateral position of the vehicle for each of the state transition matrix approximations is compared against the current lateral position of the vehicle,

Table 3.1: Vehicle parameters of 1989 GMC 2500 pick-up truck.

Symbol	Value	Unit
m	3255	kg
a	1.895	m
b	1.459	m
h	1.234	m
T	1.615	m
$C_{\alpha f}$	-120,000	N/rad
$C_{\alpha r}$	-120,000	N/rad
I_{xx}	1830	kg-m^2
I_{yy}	6488	kg-m^2
I_{zz}	7913	kg-m^2

which has been artificially shifted into the past by the preview time. Shifting the current lateral position into the past by the preview time designates the "correct" previewed lateral position. Figures 3.1, 3.2, and 3.3 show this relationship for preview intervals of 0.5 seconds, 0.75 seconds, and 1.0 seconds respectively.

As can be seen, a shorter preview interval results in better agreement between the previewed lateral position and the "correct" lateral position. This is an intuitive relationship, as it is more difficult for the system to predict the vehicle states farther in the future. It should also be noted that for greater longitudinal velocities and more aggressive steering maneuvers, the previewed lateral position will not agree as well. In these circumstances, a shorter preview interval may prove to be necessary. The MATLAB simulations indicate that the numerical approximation of the state transition matrix provides the closest match to the "correct" previewed lateral position. Therefore, only the numerical approximation will be presented in following sections to prevent overcrowded plots.

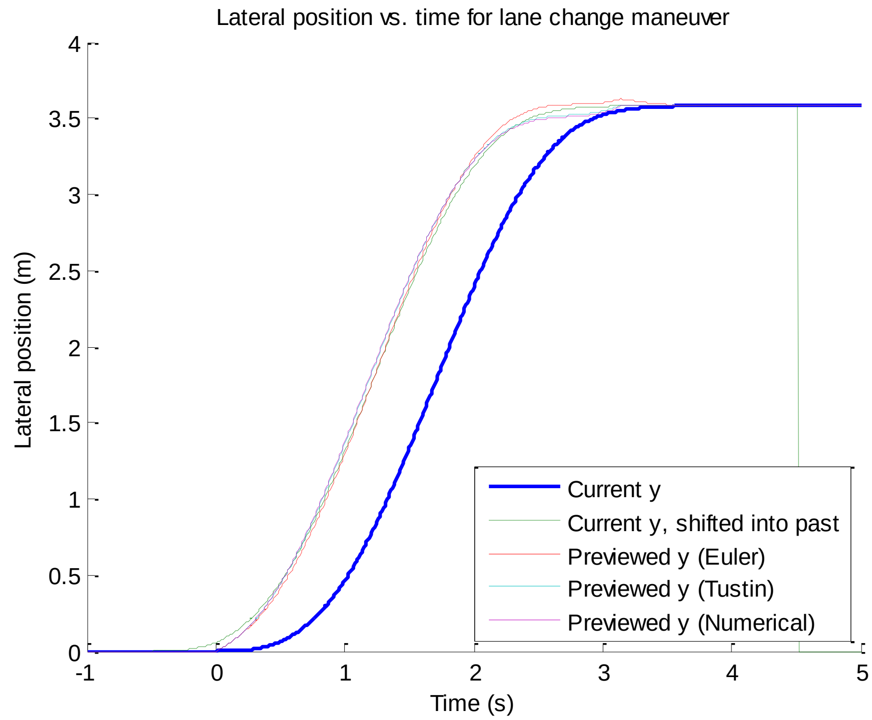

Figure 3.1: Comparison of previewed lateral positions for preview interval of 0.5 sec.

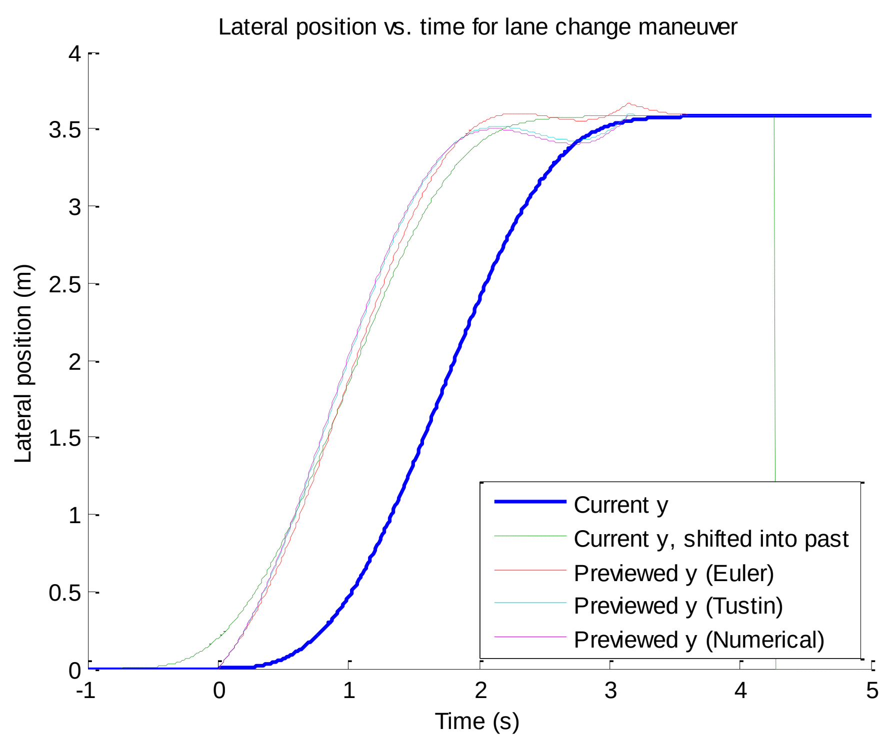

Figure 3.2: Comparison of previewed lateral positions for preview interval of 0.75 sec.

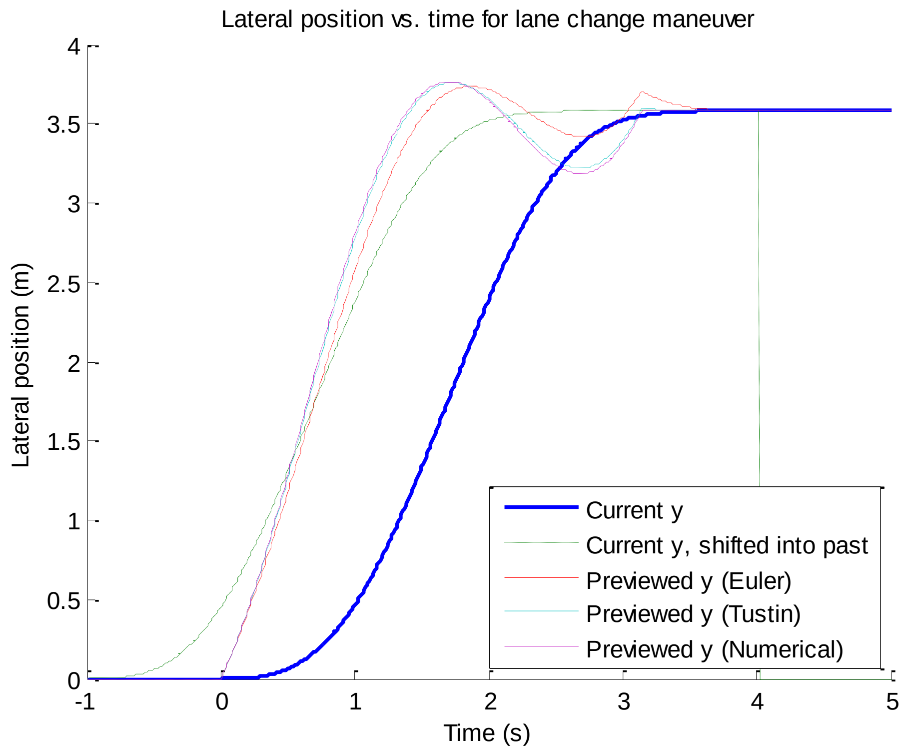

Figure 3.3: Comparison of previewed lateral positions for preview interval of 1.0 sec.

3.2 Closed-Loop Vehicle Path Following

The previous section demonstrated how to predict a vehicle's position over a specified preview interval with an open-loop steering setup. This information will now be used to develop a closed-loop controller, mathematically identical to the controller developed by MacAdam. In his work, MacAdam specified a local performance index for the vehicle's lateral position of the form

$$J \triangleq \frac{1}{T}\int_{t}^{t+T} \{[f(\eta) - y(\eta)]W(\eta - t)\}^2 \, d\eta \tag{3.12}$$

where f is the previewed input, y is the previewed output, T is the preview time, and W is an arbitrary weighting function over the preview interval. Minimizing this performance index reduces the error between the previewed input (the road) and the previewed output (the predicted vehicle path), as seen in Figure 3.4, and results in the optimal control of the system. If the weighting function is specified as the Dirac delta function where all preview information is taken at the preview time, MacAdam shows that the optimal control is given by

$$u^0(t) = \frac{f(t+T) - y(t+T)}{TK} \tag{3.13}$$

where

$$K \triangleq C^T \left[I + \sum_{n=1}^{\infty} \frac{A^n T^n}{(n+1)!} \right] B \tag{3.14}$$

Essentially, this input is the optimal steering from the controller to best maintain path-following. A block diagram of the controller function can be seen in Figure 3.5.

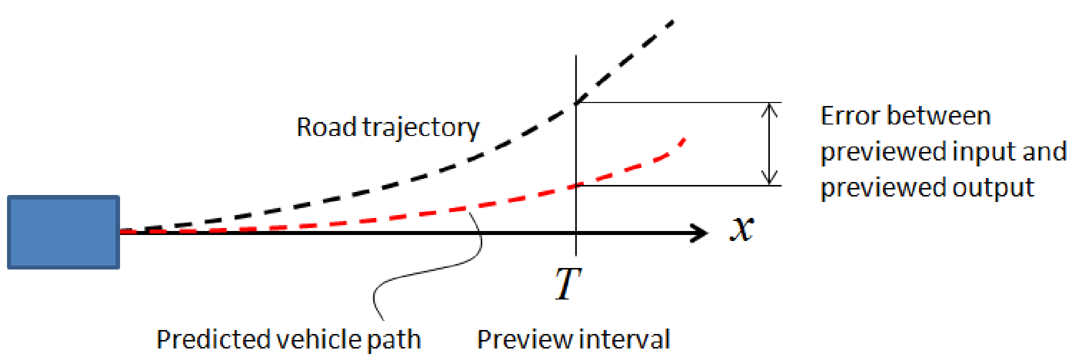

Figure 3.4: Controller error between predicted road and predicted vehicle path.

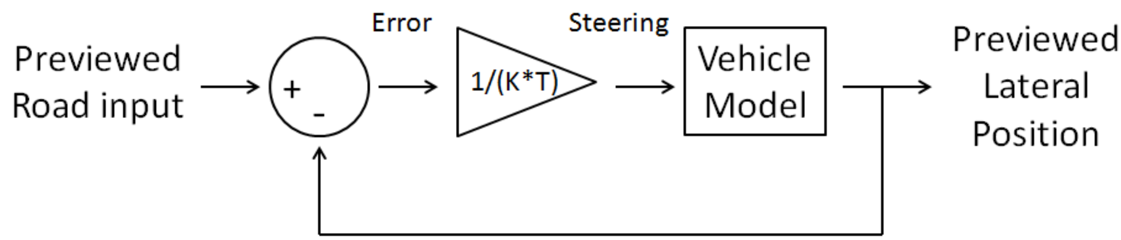

Figure 3.5: Block diagram for MacAdam controller.

MATLAB simulations were performed to test the performance of the controller. A standard sinusoidal lane change road of amplitude 3.5 m and frequency 1 rad/s (lane change over 3 seconds) was used as the input. Once again, the longitudinal velocity of 13.5 m/s (30 mph) is assumed to remain constant throughout the maneuver. It is also assumed that information about the road is known to the controller, as in the form of stored GPS data in the vehicle's computer. Therefore, the vehicle "knows" where the road will be at the preview time, shown in the simulation as the previewed road. Simulations were performed for preview intervals of 0.5 seconds, 0.75 seconds, and 1.0 seconds in Figures 3.6, 3.7, and 3.8 respectively.

The results show that the controller performs fairly well at keeping the vehicle on the desired trajectory, even for preview times up to 1.0 second. Although the vehicle overshoots the desired trajectory, it remains within the bounds of the lane in all cases (average lane width of 3.5 m, as defined by the Federal Highway Administration [3] is assumed).

The conditions used in this section do not represent an emergency maneuver; the aggressiveness of the road input is based on a standard lane change over 3 seconds at any given speed. An emergency steering maneuver would be more aggressive and

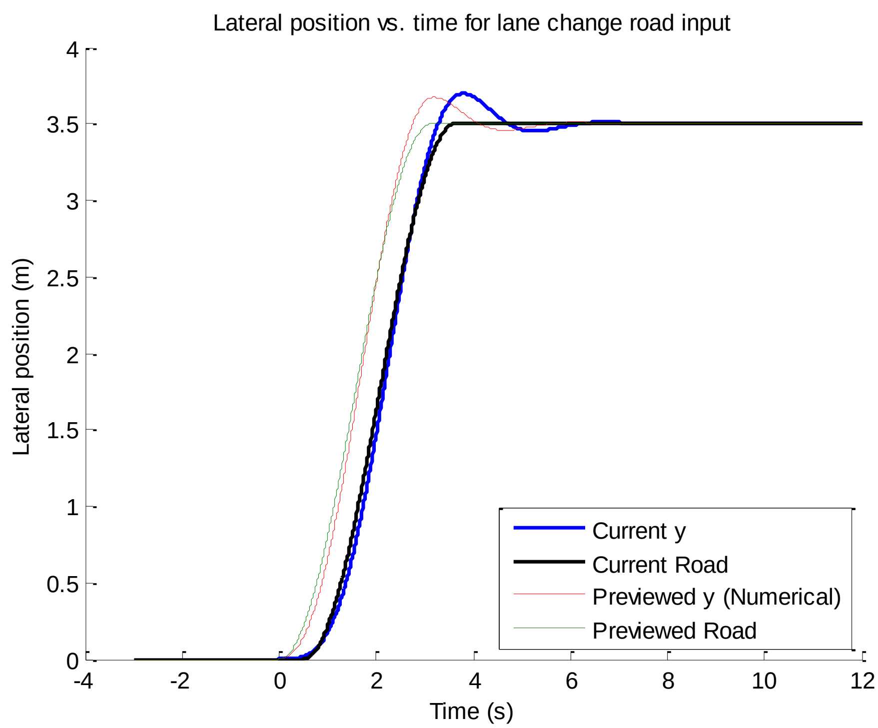

Figure 3.6: Performance of controller for preview interval of 0.5 sec.

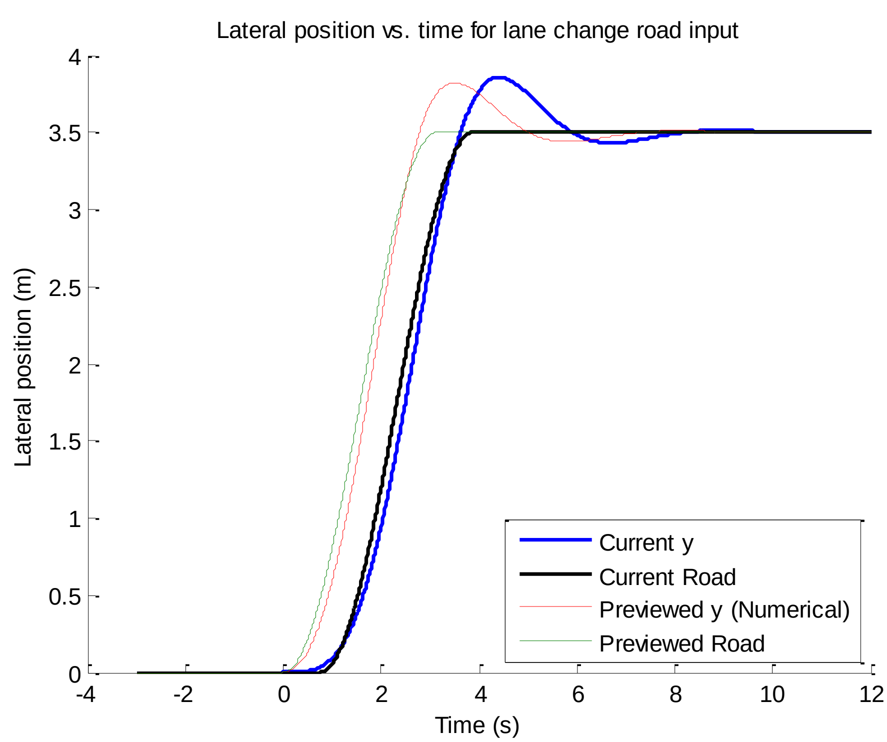

Figure 3.7: Performance of controller for preview interval of 0.75 sec.

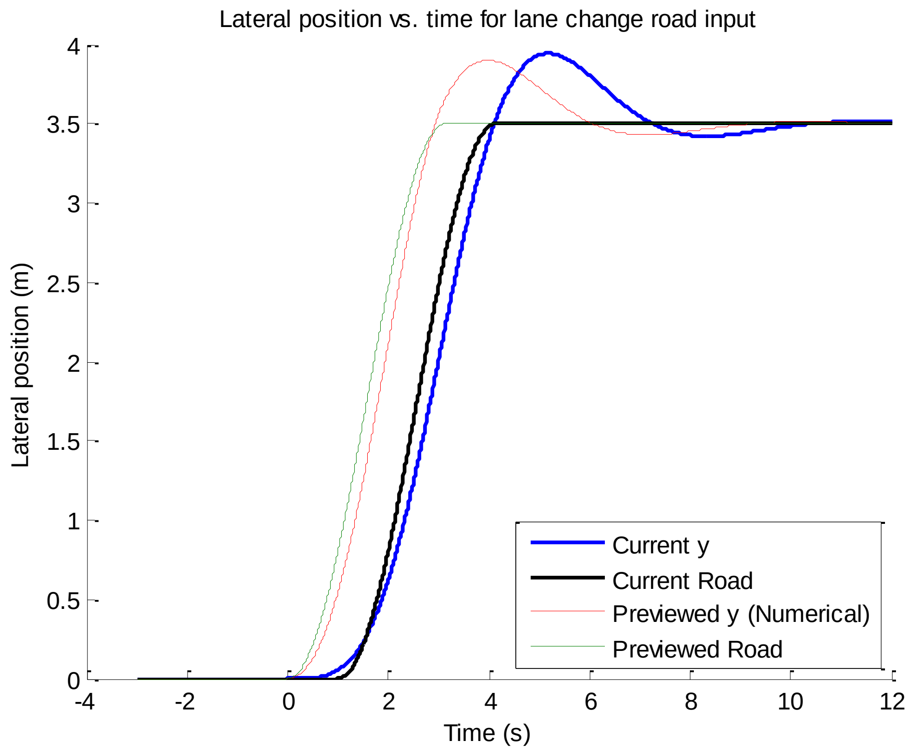

Figure 3.8: Performance of controller for preview interval of 1.0 sec.

result in a more under-damped system with greater overshoot. An emergency situation will be explored in Chapter 4 when rollover is considered.

3.3 Closed-Loop Path Following with Bank Angle

This section now explores the inclusion of bank angle within the closed-loop system. The model now considers bank angle as an explicit input in the linear system, as seen in the block diagram of Figure 3.9. Here, the bank angle of the terrain is assumed to remain constant. A constant bank angle would be present in driving situations when the vehicle is going around a highway turn or when the vehicle has left the road and is driving on the shoulder or median. As derived in Chapter 2, the B matrix of the state space bicycle model then becomes

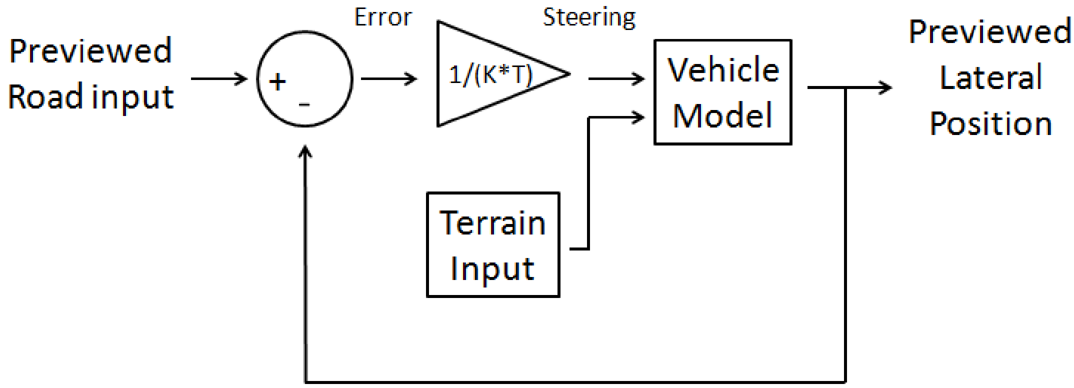

Figure 3.9: Block diagram for controller with bank angle input.

$$B = \begin{bmatrix} 0 & 0 \\ \dfrac{-C_{\alpha f}}{m} & g \\ \dfrac{-aC_{\alpha f}}{I_{zz}} & 0 \\ 0 & 0 \end{bmatrix} \tag{3.15}$$

MATLAB simulations were performed for the same vehicle parameters as the previous section, with the addition of a severe 8-degree bank angle, equivalent to a 14% superelevation. Once again, a sinusoidal lane change road input was used in two scenarios: the vehicle turns up the slope during the lane change (Figure 3.10) and the vehicle turns down the slope during the lane change (Figure 3.11). Both simulations used a preview interval of one second.

The results show that the controller is able to maintain path following, even with the addition of a constant terrain bank angle. The overshoot is slightly greater in the case when the vehicle turns down the slope, but the vehicle is still able to stay within the bounds of the lane.

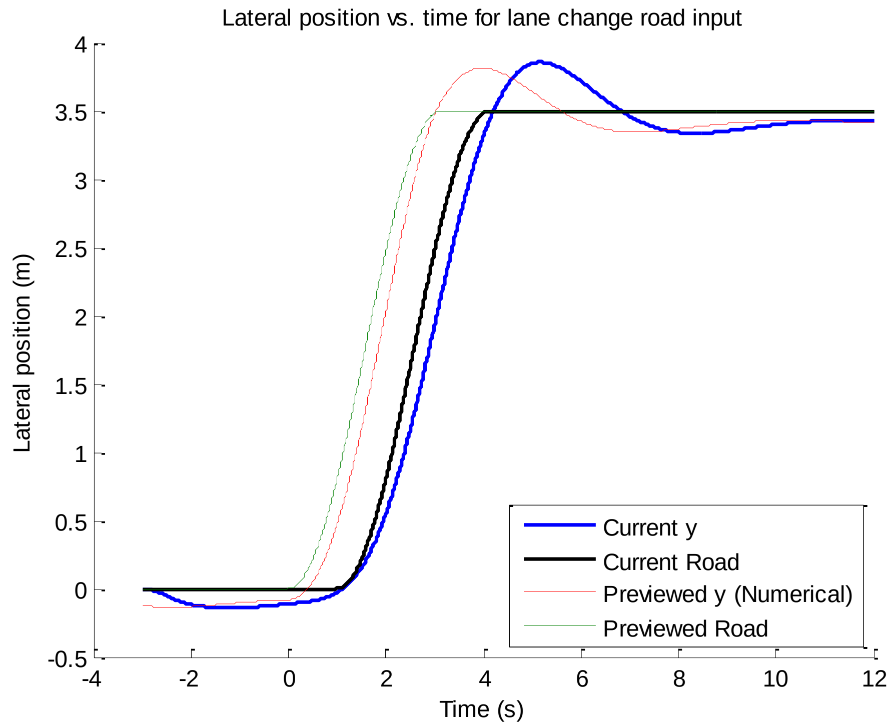

Figure 3.10: Controller performance for 14% superelevation bank angle (turning up the slope).

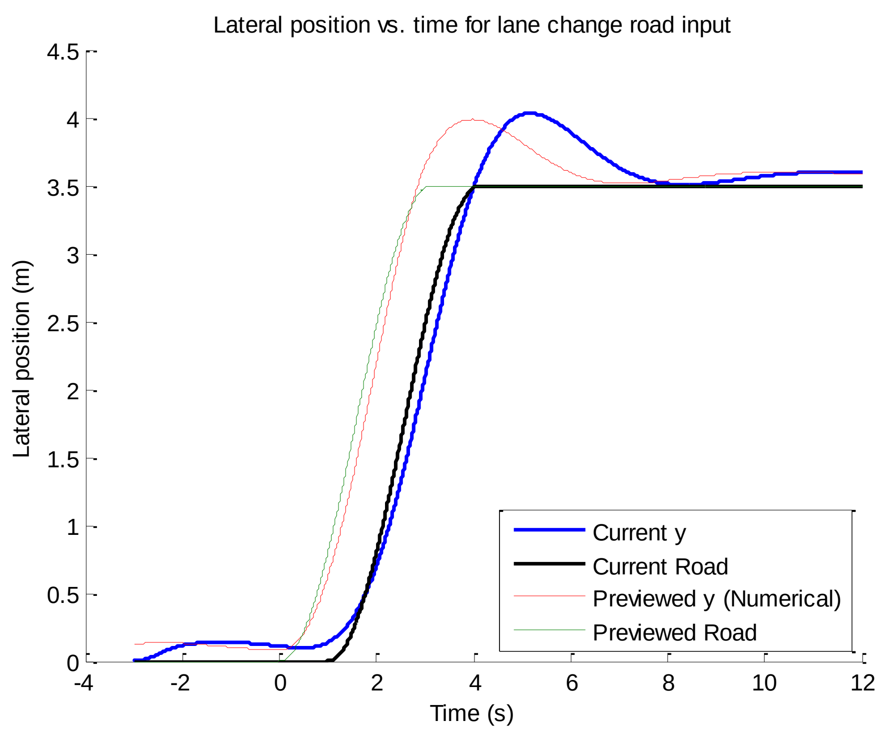

Figure 3.11: Controller performance for 14% superelevation bank angle (turning down the slope).

Another interesting scenario considers when the driver model does not have prior knowledge of the terrain bank angle. Therefore, although the model accounts for the terrain's influence on vehicle dynamics, it is here assumed that the driver is unable preview the bank angle on the road. To simulate this situation, the terrain input column of the previewed B matrix was set to zero in the form

$$B_{preview} = \begin{bmatrix} \mathrm{x} & 0 \\ \mathrm{x} & 0 \\ \mathrm{x} & 0 \\ \mathrm{x} & 0 \end{bmatrix} \tag{3.16}$$

The controller performance when the driver model does not have knowledge of the terrain bank angle is seen in Figure 3.12. Once again, a preview time of one second was used. Unable to predict the bank angle, the plot shows that the lateral position has greater bias down the slope of the terrain. This results from the fact that the driver model does not provide the correct steering input to compensate for the bank angle. A similar effect would also occur if information about the terrain gathered from the vehicle's sensors was incorrect.

Even without this knowledge, the vehicle is able to maintain path-following and stay within the bounds of the lane, as seen in Figure 3.13. In this image, the plot of Figure 3.12 has been overlaid with representations of the standard lane width of 3.5 m and the vehicle's track width of 1.6 m.

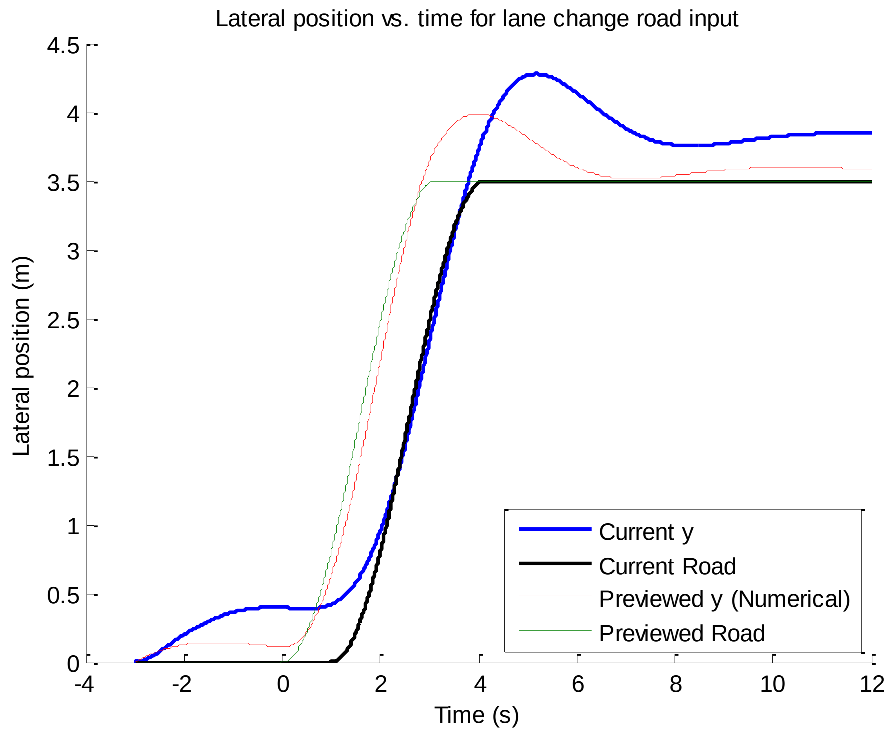

Figure 3.12: Controller performance without preview of terrain effects.

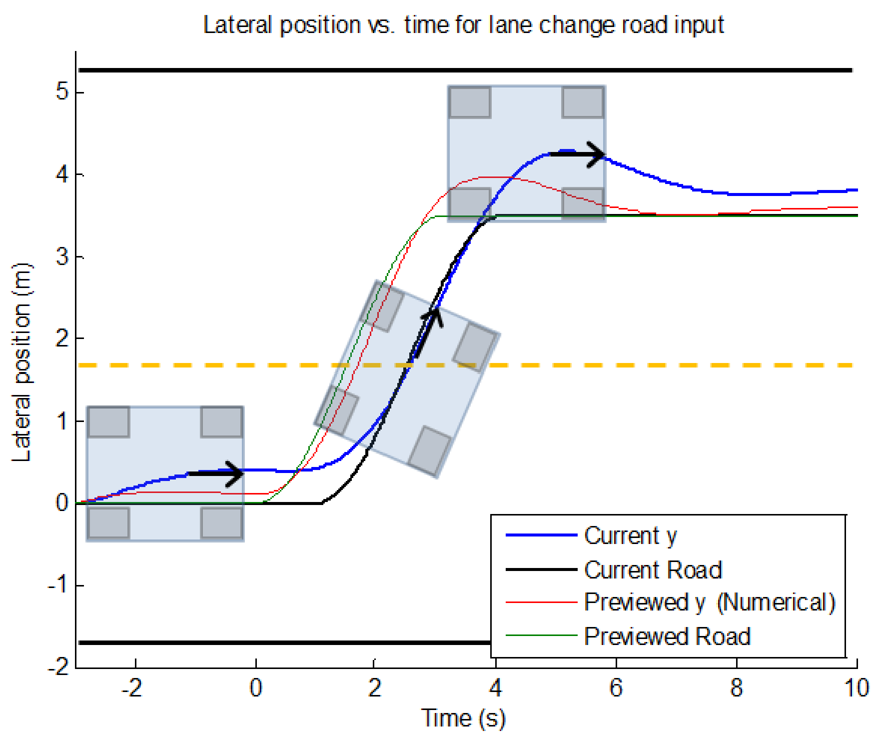

Figure 3.13: Controller performance overlaid with vehicle width and lane width.

3.4 References

[1] MacAdam, C. C. "Application of an Optimal Preview Control for Simulation of Closed-Loop Automobile Driving," *IEEE Transactions on Systems, Man, and Cybernetics*, SMC-11(6), pp. 393-399, 1981.

[2] F. Golnaraghi and B. Kuo, Automatic Control Systems, 9th ed. New York: John Wiley & Sons, Inc. 2010.

[3] DOT, "Mitigation Strategies for Design Exceptions - Lane Width," *U.S. Department of Transportation: Federal Highway Administration*, July 2007.

Chapter 4 - Detection of Rollover

This chapter focuses on introducing the concept of the Zero-Moment Point (ZMP) [1-5] as a vehicle rollover metric. The ZMP is then used to predict an impending rollover event in the future during a worst-case driving scenario using the same methods presented in Chapter 3. The results of the vehicle model are also compared to predictions from the commercial driving software CarSim. Finally, tire lag effects are considered to determine if they affect the roll predictions.

4.1 Concept of Zero-Moment Point

As discussed previously, the zero-moment point is defined as the point on the ground where the summation of the tipping moments acting on an object, due to gravity and inertia forces, equals zero [6]. If this point moves outside the object's support polygon, the object will overturn. This concept can be applied to a general object for further understanding. Figure 4.1(a) shows a mass resting on a tilt table. The table is assumed to have enough friction that the mass does not slip. In Figure 4.1(a), the reaction force $\vec{N}$ lies directly below the object's center of mass. The point where this reaction acts is the ZMP. As the object is progressively inclined as seen in Figure 4.1(b), 4.1(c), and 4.1(d), the reaction force shifts to the right to balance the moment created by gravity and satisfy the definition of ZMP. Once the table is tilted to an angle that the ZMP is located outside the object's contact polygon as seen in Figure 1.4(d), the object is no longer stable and will overturn.

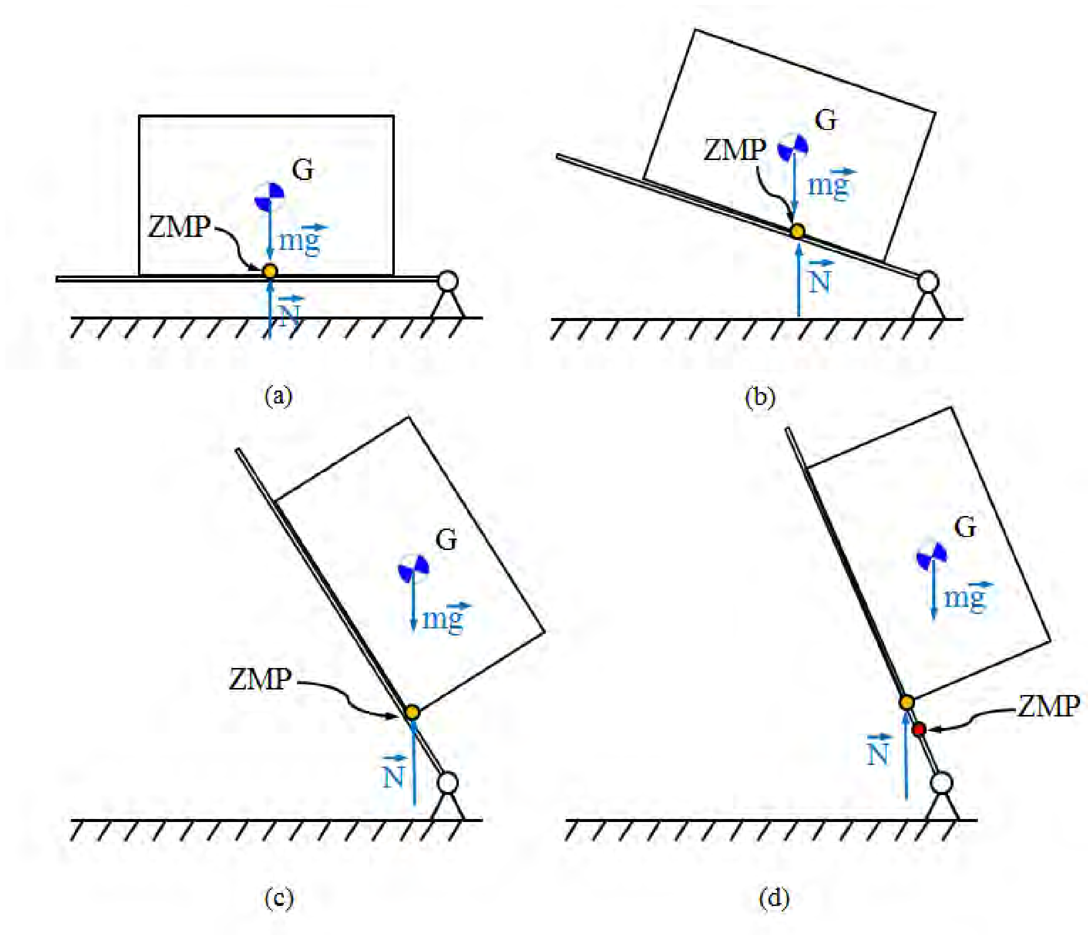

Figure 4.1: Free-body diagrams of mass on a tilt table [3].

Applying the concept of the zero-moment point as a vehicle rollover metric presents several advantages. One advantage of the ZMP is that it explicitly considers terrain effects in its derivation. Another one of its more significant advantages is that calculation of the ZMP does not rely on knowledge of the vehicle-ground contact forces. By treating the vehicle as a kinematic chain, it is possible to calculate each body's net moment contribution to the zero-moment point. This calculation only requires measurement of the kinematic motion of all objects in the chain, information that is accessible through inertial measurement units and knowledge of the vehicle parameters.

Although the location of the zero-moment point exists in three-dimensional space, only the coordinate of its lateral position on the ground from the vehicle centerline, called y_{ZMP}, is necessary for the application to vehicle rollover. In a vehicle, the contact polygon is defined where the four tires touch the ground. The distance of y_{ZMP} from the edge of the contact polygon is used as the metric for the vehicle's rollover propensity. If y_{ZMP} is located outside the track width of the vehicle, the vehicle will begin to overturn.

4.2 Formulation of Zero-Moment Point

The derivation for the location of the ZMP within a vehicle will now be presented. Consider the general kinematic chain shown in Figure 4.2. The ith body of the kinematic chain has a mass m_i and an inertia tensor $\mathbf{I}_i$ about its center of mass. It is also assumed that this body has a translational velocity $\vec{v}_i$, a translational acceleration $\vec{a}_i$, an angular velocity $\vec{\omega}_i$, and an angular acceleration $\vec{\alpha}_i$. Using the general equations of motion of the chain [7-9] and D'Alembert's principle [10], the moment equation about point A in Figure 4.2 can be written as

$$\vec{M}_A = \sum_i (\vec{p}_i \times m_i \vec{a}_i) + \sum_i (\mathbf{I}_i \, \vec{\alpha}_i + \vec{\omega}_i \times \mathbf{I}_i \vec{\omega}_i) - \sum_i (\vec{p}_i \times m_i \vec{g}) \tag{4.1}$$

where $\vec{p}_i = \vec{r}_i - \vec{r}_{ZMP}$. Point A then becomes the zero-moment point when $\vec{M}_A$ = [0 0 M_z]$^{\mathrm{T}}$.

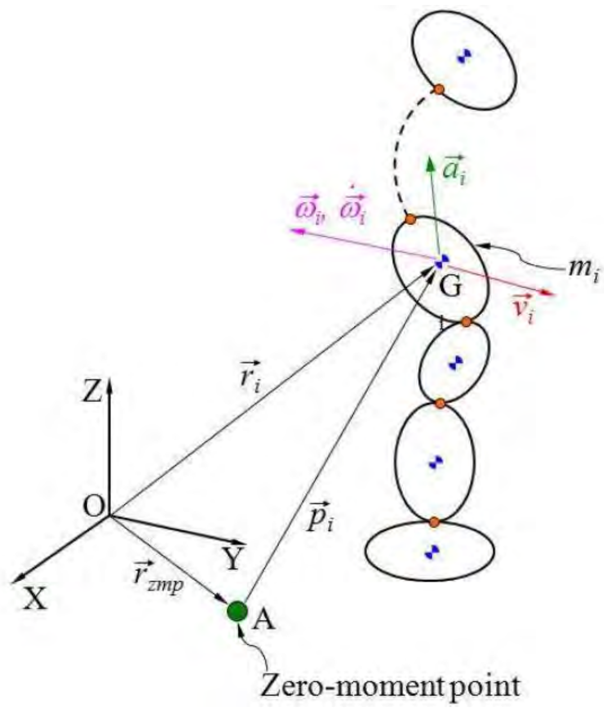

Figure 4.2: Generalized kinematic chain [3].

This generalized moment equation can be applied to the two-degree-of-freedom bicycle model. Previous work by the IVSG research group at Penn State [3] derived the ZMP for both the two-degree-of-freedom bicycle model and the three-degree-of-freedom roll model. The results of the two models proved to be nearly identical; therefore, the y_{ZMP} derivation will only be done for the simpler bicycle model.

The symbols and nomenclature used in the derivation are shown in Table 4.1. Figure 4.3 shows the two-degree-of-freedom model on a terrain bank angle. The location of the zero-moment point is given by the vector

$$\vec{r}_{ZMP} = x_{ZMP}\hat{\imath} + y_{ZMP}\hat{\jmath} + z_{ZMP}\hat{k} \tag{4.2}$$

Table 4.1: y_{ZMP} nomenclature.

Parameter	Definition
m	Vehicle mass
I_{xx}	Mass moment of inertia about vehile x-axis
I_{yy}	Mass moment of inertia about vehicle y-axis
I_{zz}	Mass moment of inertia about vehicle z-axis
I_{xz}	Mass product of inertia about CG
I_{yz}	Mass product of inertia about CG
a	Distance from CG to front axle along the x-axis
b	Distance from CG to rear axle along x-axis
h	Height of CG from the base of the wheels
T	Track width of vehicle
ϕ_t	Bank angle of terrain
ϕ_r	Roll angle of vehicle
θ	Pitch angle of vehicle
ψ	Yaw angle of vehicle
p	Roll rate of vehicle
q	Pitch rate of vehicle
r	Yaw rate of vehicle
α_x	Roll acceleration of vehicle
α_y	Pitch acceleration of vehicle
α_z	Yaw acceleration of vehicle
$a_{Gx,y,z}$	Acceleration of CG in x-, y-, and z-direction

Given the definition that the zero-moment point must lie on the ground, z_{ZMP} can be expressed in terms of the terrain and vehicle properties given in Figure 4.3. For the case of Figure 4.3 in which $\phi_r > \phi_t$, it can be shown that

$$z_{ZMP} = h + \left(\frac{T}{2} - y_{ZMP}\right) \tan\left(\phi_r - \phi_t\right) \tag{4.3}$$

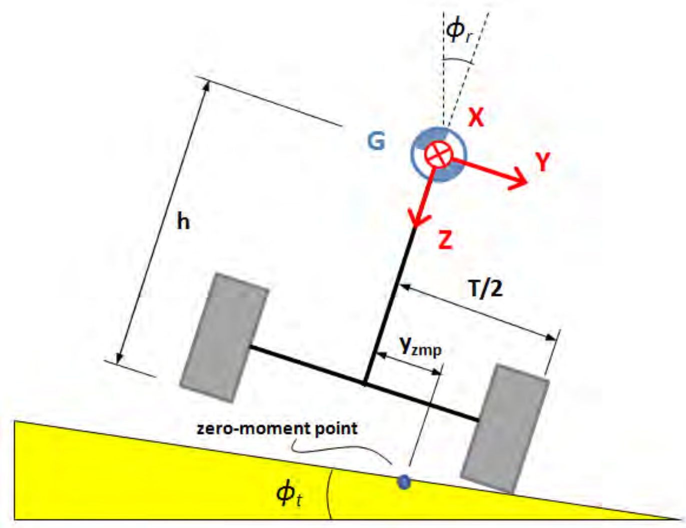

Figure 4.3: Bicycle model on banked terrain, $\phi_r > \phi_t$.

It can also be shown for the case where $\phi_r < \phi_t$ that

$$z_{ZMP} = h + \left(\frac{T}{2} + y_{ZMP}\right)\tan\left(-\phi_r + \phi_t\right) \tag{4.4}$$

Unifying Equations 4.3 and 4.4 to account for both conditions results in the following:

$$z_{ZMP} = h + \frac{T}{2}\left|\tan\left(\phi_r - \phi_t\right)\right| - y_{ZMP}\tan\left(\phi_r - \phi_t\right) \tag{4.5}$$

This results in the location of the zero-moment point expressed as

$$\vec{r}_{ZMP} = x_{ZMP}\hat{\imath} + y_{ZMP}\hat{\jmath} + \left[h + \frac{T}{2}\left|\tan\left(\phi_r - \phi_t\right)\right| - y_{ZMP}\tan\left(\phi_r - \phi_t\right)\right]\hat{k} \tag{4.6}$$

Now that the vector location of the zero-moment point is defined in terms of y_{ZMP} and x_{ZMP}, the remaining terms of Equation 4.1 can be discussed. In the case of the bicycle model, the coordinate system is located at the vehicle's center of gravity. This means that $\vec{r}_i = 0$ and that $\vec{p}_i = -\vec{r}_{ZMP}$.

The vehicle's motion is not constrained in any direction; therefore the angular velocity, angular acceleration, and linear acceleration at the center of gravity can be expressed as

$$\vec{\omega} = p\hat{\imath} + q\hat{\jmath} + r\hat{k} \tag{4.7}$$

$$\vec{\alpha} = \alpha_x\hat{\imath} + \alpha_y\hat{\jmath} + \alpha_z\hat{k} \tag{4.8}$$

$$\vec{a}_G = a_{Gx}\hat{\imath} + a_{Gy}\hat{\jmath} + a_{Gz}\hat{k} \tag{4.9}$$

Looking at the properties of the vehicle, an inertia tensor can be defined as the following:

$$\mathbf{I} = \begin{bmatrix} I_{xx} & 0 & -I_{xz} \\ 0 & I_{yy} & -I_{yz} \\ -I_{xz} & -I_{yz} & I_{zz} \end{bmatrix} \tag{4.10}$$

where $I_{xy} = 0$ due to the assumption that the vehicle is symmetric about the xz-plane. The final term in Equation 4.1 is the gravitational acceleration vector. When converted from global-fixed coordinates to body-fixed coordinates, the gravitational acceleration vector takes the form

$$\vec{g} = -g\sin(\theta)\hat{\imath} + g\sin(\phi_r)\cos(\theta)\hat{\jmath} + g\cos(\phi_r)\cos(\theta)\hat{k} \tag{4.11}$$

Substituting Equations 4.6 - 4.11 into Equation 4.1 and setting the x and y components equal to zero (due to the fact that $\vec{M}_A = [0\ 0\ M_z]^{\mathrm{T}}$) allows y_{ZMP} to be solved for in the form

$$
\begin{aligned}
y_{ZMP} = \{ & mg\cos(\theta)\sin(\phi_r)\,[T|\tan(\phi_r - \phi_t)| + 2h] \\
& - ma_{Gy}[T|\tan(\phi_r - \phi_t)| + 2h] - 2I_{xx}\alpha_x + 2I_{xz}\alpha_z \\
& + 2I_{yz}(q^2 - r^2) + 2\big(I_{xz} + I_{yy} - I_{zz}\big)qr \} \\
& / \{ 2m\big[g\cos(\theta)\cos(\phi_t)\sec(\phi_r - \phi_t) \\
& - a_{Gy}\tan(\phi_r - \phi_t) - a_{Gz}\big] \}
\end{aligned}
\tag{4.12}
$$

A linearized equation of the rigid model-derived y_{ZMP}, found in [5], is expressed as:

$$
y_{ZMP} = -\frac{I_{xx}}{mg}(\ddot{\phi}_t + \ddot{\phi}_r) + h_{sr}(\phi_t + \phi_r) - \frac{h_{sr}}{g}a_{Gy} \tag{4.13}
$$

where h_{sr} is the height of the sprung mass center of gravity from the roll center as defined in Table 2.2 and ϕ_r is the roll angle of the sprung mass. Because the y equations for both the rigid vehicle model and the roll model produce nearly identical results when applied to a real vehicle, the simpler form of the y equation given in Equation 4.13 is applied to the roll model for this study.

4.3 Inclusion of y_{ZMP} in Vehicle Model

Now that the equation for y_{ZMP} has been derived, it can be added as an output of the state space model. Equation 4.13 can be written in terms of the vehicle states of the three-degree-of-freedom roll model without tire lag (tire lag effects are explored in Section 4.6). The state vector used for the roll model is given as

$$
x = \begin{bmatrix} y \\ V \\ r \\ \dot{\phi} \\ \phi \\ \psi \end{bmatrix} \tag{4.14}
$$

where y and ψ have been added to the ends of the state vector as shown in Chapter 3. Recognizing the general state space notation of

$$\dot{x} = Ax + Bu \tag{4.15}$$

the roll acceleration and lateral acceleration can be written in terms of the A and B matrices of the roll model in the form

$$\ddot{\phi}_r = [0 \quad 0 \quad 0 \quad 1 \quad 0 \quad 0][Ax + Bu] \tag{4.16}$$

$$a_y = [0 \quad 1 \quad 0 \quad 0 \quad 0 \quad 0][Ax + Bu] + Ur \tag{4.17}$$

Similarly, Equation 4.13 can then be written in terms of the A and B matrices of the roll model in the form

$$y_{ZMP} = \left[0 \quad -\frac{h_{sr}}{g} \quad 0 \quad -\frac{I_{xx}}{mg} \quad 0 \quad 0\right][Ax + Bu] + h_{sr}(\phi_t + \phi_r - \frac{Ur}{g}) \tag{4.18}$$

where $\ddot{\phi}_t = 0$ due to the assumption that the terrain bank angle is constant.

4.4 Inclusion of Previewed y_{ZMP} in Vehicle Model

Prediction of y_{ZMP} is possible using the same methods that were used to predict the vehicle's lateral position in Chapter 3. Equation 4.18 is capable of calculating the vehicle's rollover propensity at the current time. To prevent a rollover event, however, possibly in the form of an early warning system or corrective action, it is necessary to predict the vehicle's rollover propensity over the preview time based on the current states and inputs.

The state vector at the preview time, T, was given in Chapter 3 as

$$x(t+T) = \Phi(t+T,t)x(t) + \Psi TBu \tag{4.19}$$

where

$$\Psi = I + \sum_{k=1}^{\infty} \frac{(TA)^k}{(k+1)!} \tag{4.20}$$

Once again, it should be noted that Equation 4.20 does not quickly converge when elements of the A matrix are large. An alternate method of calculating the previewed input coefficient for these situations is presented in Section 4.6. The numerical approximation of the state transition matrix is used because it provides the best accuracy, hereafter referred to as the discrete A matrix, A_d. Similarly, the previewed approximation of the input term is hereafter referred to as the discrete B matrix, B_d, such that

$$A_d = \Phi_{num}(t+T,t) \tag{4.21}$$

$$B_d = \Psi TB \tag{4.22}$$

and Equation 4.19 is written as

$$x(t+T) = A_d x(t) + B_d u \tag{4.23}$$

Now that the previewed state vector is once again defined, Equation 4.18 can be previewed. Roll acceleration at the preview time is given by

$$\ddot{\phi}_{r,p} = [0 \quad 0 \quad 0 \quad 1 \quad 0 \quad 0][Ax(t+T) + Bu(t+T)] \tag{4.24}$$

Recognizing that all inputs are assumed constant over the preview interval such that $u(t+T) = u(t)$ and substituting Equation 4.23 gives

$$\ddot{\phi}_{r,p} = [0 \quad 0 \quad 0 \quad 1 \quad 0 \quad 0][A[A_d x + B_d u] + Bu] \tag{4.25}$$

Similarly, the previewed roll angle and previewed lateral acceleration can be written in this manner as

$$\phi_{r,p} = [0 \quad 0 \quad 0 \quad 0 \quad 1 \quad 0][A_d x + B_d u] \tag{4.26}$$

$$\begin{aligned} a_{y,p} = [0 \quad 1 \quad 0 \quad 0 \quad 0 \quad 0][A[A_d x + B_d u] + Bu] \\ + U[0 \quad 0 \quad 1 \quad 0 \quad 0 \quad 0][A_d x + B_d u] \end{aligned} \tag{4.27}$$

Substituting Equations 4.25, 4.26, and 4.27 into Equation 4.13 gives y_{ZMP} at the preview time as

$$\begin{aligned} y_{ZMP}(t+T) = \left[0 \quad -\frac{h_{sr}}{g} \quad 0 \quad -\frac{I_{xx}}{mg} \quad 0 \quad 0\right][A[A_d x + B_d u] + Bu] \\ + \left[0 \quad 0 \quad -\frac{h_{sr}U}{g} \quad 0 \quad h_{sr} \quad 0\right][A_d x + B_d u] + h_{sr}\phi_t \end{aligned} \tag{4.28}$$

Just as in the case of previewed lateral position, Equation 4.28 can be used to add the previewed y_{ZMP} as an output of the state-space vehicle model.

4.5 Rollover Prevention with Corrective Steering

An important application of previewed y_{ZMP} could be to detect when a driver's present steering input will soon result in wheel lift. By identifying impending rollover in the near future, warnings or corrective steering inputs can be applied to mitigate the risk. For implementation of this approach, it is necessary to determine the minimum preview time needed to predict and prevent a rollover event. This section examines the use of previewed y_{ZMP} to determine the necessary preview time to prevent rollover.

A worst-case driving situation as defined in [5] was considered for the MATLAB simulation in order to maximize the vehicle's rollover propensity. The parameters for the 1989 GMC 2500 pick-up truck, introduced in Chapter 3, were used due to the vehicle's high center-of-gravity. A highway speed of 26.8 m/s (60 mph) was used, as well as the introduction of an 8-degree bank angle (14% superelevation), a value representative of the designed bank angle in a sharp highway curve. The steering input was designed so that the vehicle turns up the slope of the terrain. This driving scenario is not uncommon; a vehicle that travels onto the shoulder or median of a highway would experience similar circumstances and a similar steering input as the driver tried to correct his/her path.

4.5.1 Corrective Steering Maneuver #1

Ultimately, closed-loop control is intended for wheel-lift prevention; however, the preview horizon is best examined and understood using open-loop analysis. To this end, a simple open-loop steering maneuver was used as the input, where the steering angle of the tires follows a sinusoidal path to the desired steering magnitude and then remains constant in the form:

$$\delta_f = \begin{cases} \frac{A}{2} * \sin\left(2\pi f t - \frac{\pi}{2}\right) + \frac{A}{2} & \text{for } 0 < t \leq \frac{\pi}{f} \\ A & \text{for } t > \frac{\pi}{f} \end{cases} \tag{4.29}$$

where A is the steering angle magnitude, and f is the steering frequency. The rollover prevention control considered here is simple as well and also open-loop in nature. If the system detects that previewed y_{ZMP} has gone outside the vehicle's track width (indicating wheel lift), it will implement a corrective steering input where the steering angle of the tires follows a sinusoidal path (of the same frequency) from its current value back to a zero steering input in the form:

$$\text{if } y_{ZMP}(t+T) \geq \frac{T_r}{2} \text{ at } t = t^*,$$

$$\delta_f = \begin{cases} \frac{A}{2} * \sin\left(2\pi f t + \frac{\pi}{2}\right) + \frac{A}{2} & \text{for } t^* < t \leq t^* + \frac{\pi}{f} \\ 0 \quad \text{for } t > t^* + \frac{\pi}{f} \end{cases} \tag{4.30}$$

where T_r is the track width of the vehicle. Figure 4.4 shows a graphical example of corrective steering maneuver #1. Various steering angles and frequencies were considered to determine the preview time needed to prevent wheel lift. It is assumed that there is no tire skidding for the given maneuvers. Previous work by the IVSG research group [5] showed that wheel lift will occur before the tires skid for steering frequencies below 0.8 Hz. Therefore, results for steering frequencies above this value should be considered questionable as skidding is likely to precede rollover.

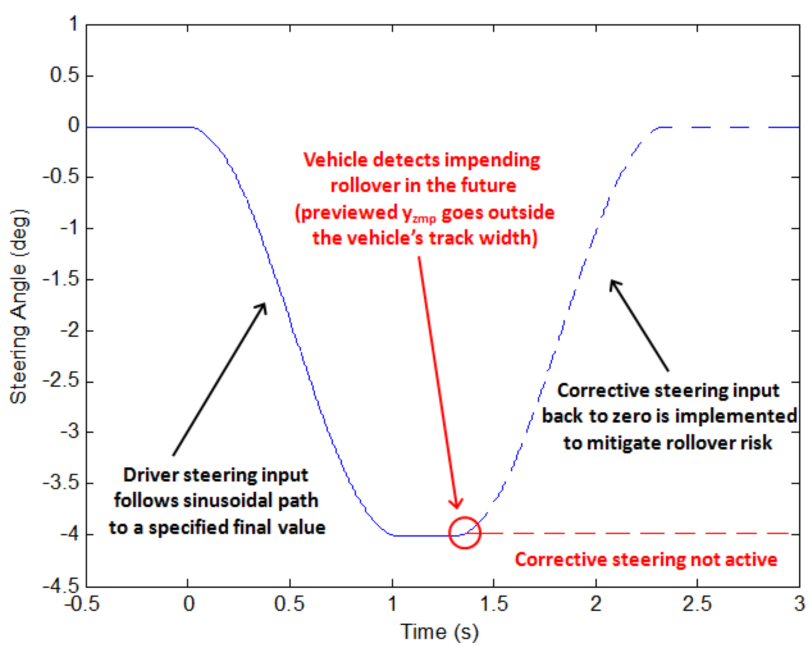

Figure 4.4: Example corrective steering maneuver #1.

To understand how the aggressiveness of the driver's steering input affects the preview time needed for a successful corrective maneuver, the limiting preview time to prevent wheel lift was calculated for various driver steering inputs. For this study, y_{ZMP} has been normalized such that values greater than 1 or less than -1 represent wheel lift. The minimum acceptable preview time was determined as follows: for each combination of steering angle and steering frequency, the preview time was iteratively increased from zero until the extreme value of the normalized current y_{ZMP} fell between 0.97 and 0.98 (or -0.97 and -0.98). At this point, rollover prevention was considered to have occurred and the preview time was recorded. The vehicle simulation software, CarSim, was also used to compare the results of the linear system. In CarSim, the preview time was recorded when the vertical force of any tire fell between 200 N and 300 N (range of 2-3% of the static load on each tire), a value low enough to indicate that wheel lift is imminent. The results are shown in Figure 4.5. Representative plots showing the value of y_{ZMP} with and without corrective rollover steering at the limiting preview time can also be seen in Figure 4.6(a) and 4.6(b) respectively. These plots include y_{ZMP} for the linear system and for CarSim.

The results show that previewed y_{ZMP} information is capable of preventing rollover. When the corrective steering algorithm is active in Figure 4.6(a), the current y_{ZMP} remains within the track width of the vehicle. When the corrective steering algorithm is not active in Figure 4.6(b), the current y_{ZMP} rises well above the threshold for wheel lift. There is also very good agreement between the linear prediction of y_{ZMP} and the CarSim prediction of y_{ZMP}. The results indicate that the roll model prediction is more conservative than CarSim, as shown by the higher preview times. This is an

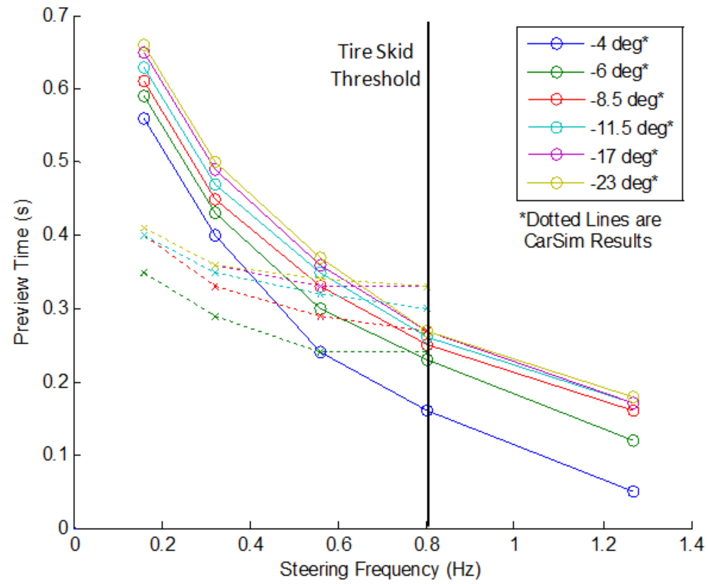

Figure 4.5: Minimum preview times required to prevent rollover; corrective steering maneuver #1.

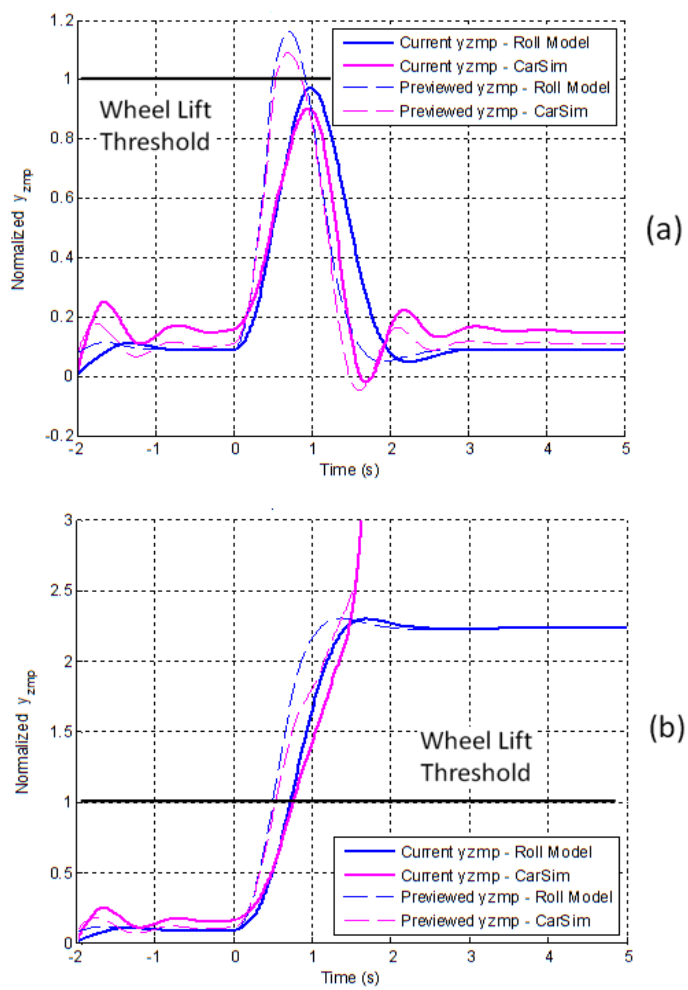

Figure 4.6: y_{ZMP} (a) with and (b) without corrective steering maneuver #1.

acceptable outcome, as it is more desirable to have a conservative system for rollover prevention. Figure 4.5 also shows that the limiting preview time for the roll model is greatly influenced by the frequency of the steering input (higher frequency means more severe steering input). The preview time is also dependent on the steering angle, although not as much as the frequency. This trend agrees with intuition: since previewed y_{ZMP} assumes a constant steering input, more severe steering inputs will result in earlier detection and correction through a previewed y_{ZMP} value that rises quickly. Impending rollover from a less severe steering input, however, will not be detected as quickly and requires more preview to correct the action. The limiting preview times for CarSim are much less affected by changes in the steering frequency and magnitude, but still remain less than the roll model preview times.

4.5.2 Corrective Steering Maneuver #2

A second scenario with a more severe corrective steering input was also simulated. All conditions and parameters remain the same, but the corrective steering input now follows a sinusoidal path to the opposite steering magnitude once impending rollover is detected. This corrective steering input opens up the possibility of the vehicle experiencing rollover on its opposite side. Therefore, if the vehicle detects impending rollover on its opposite side, it will implement a second corrective steering input back to zero in the form:

$$\text{if } y_{ZMP}(t+T) \geq \frac{T_r}{2} \text{ at } t = t^*,$$

$$\delta_f = \begin{cases} A * \sin\left(2\pi f t + \frac{\pi}{2}\right) & \text{for } t^* < t \leq t^* + \frac{\pi}{f} \\ -A \quad \text{for } t > t^* + \frac{\pi}{f} \end{cases}$$

$$\text{if } y_{ZMP}(t+T) \leq \frac{-T_r}{2} \text{ at } t = t^{**}, \tag{4.31}$$

$$\delta_f = \begin{cases} \frac{-A}{2} * \sin\left(2\pi f t + \frac{\pi}{2}\right) - \frac{A}{2} & \text{for } t^{**} < t \leq t^{**} + \frac{\pi}{f} \\ 0 \quad \text{for } t > t^{**} + \frac{\pi}{f} \end{cases}$$

Figure 4.7 shows a graphical example of corrective steering maneuver #2.

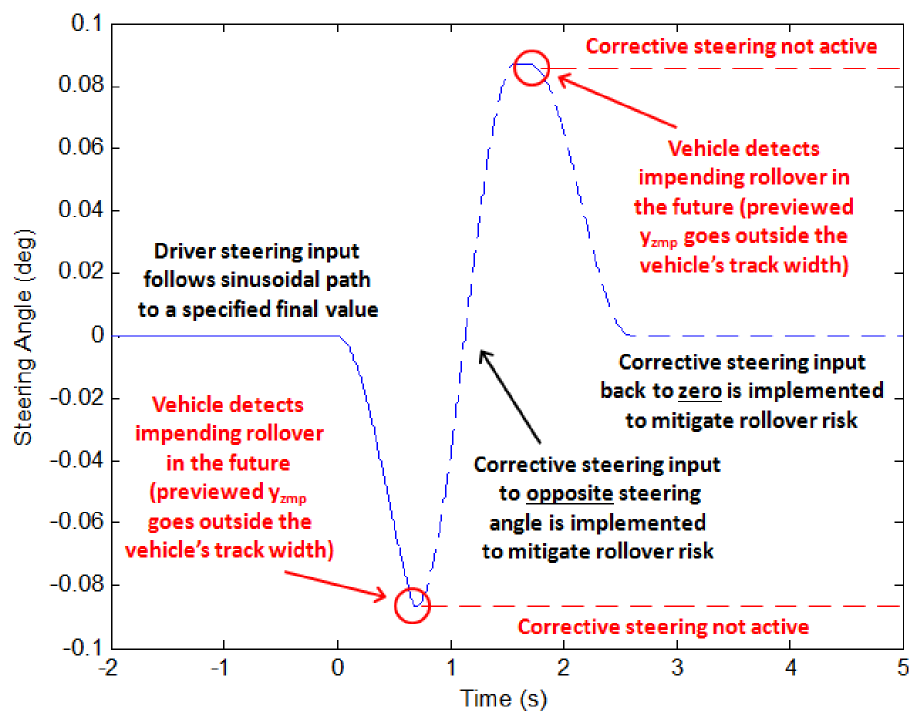

Figure 4.7: Example corrective steering maneuver #2.

Once again, various steering angles and frequencies were considered to determine the minimum acceptable preview time to prevent wheel lift. These preview times were determined with the same procedure as the previous scenario and are presented in Figure 4.8. Representative plots showing the value of y_{ZMP} with and without corrective steering at the limiting preview time can be seen in Figure 4.9(a) and 4.9(b) respectively.

As expected, slightly less preview time was required for the roll model predictions due to the more severe corrective steering input. It is interesting to note, however, that slightly longer preview times were required for the higher frequency steering inputs of the roll model and CarSim. This results from the greater overshoot of y_{ZMP} in the corrective maneuver to the opposite steering angle, where the suspension dynamics cause wheel lift on the opposite side. Although this occurrence is important, these effects are still dominated by the need for a higher preview time in the initial steering correction up the slope of the bank.

In this study, the minimum preview time needed to predict and prevent vehicle rollover was determined. The maximum required preview time for all conditions tested was found to be 0.66 sec. These results consider one particular worst-case vehicle scenario and configuration. Other vehicles and driving situations should also be tested. Limiting preview times of 0.75 sec or 1.0 sec may be used as a baseline for further study to encompass a wider variety of driving situations and provide a more conservative system. It should be noted that while a more severe corrective steering input requires slightly less preview, it also has a greater effect on the desired path of the vehicle. Further study should determine the optimal corrective steering magnitude

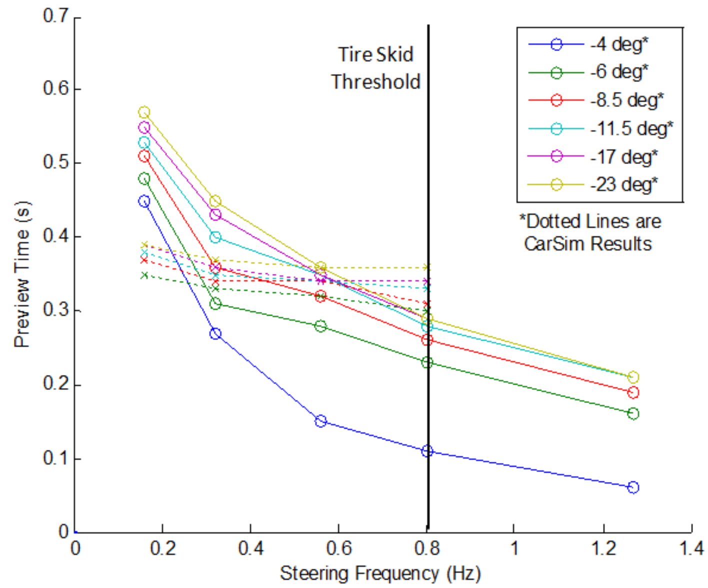

Figure 4.8: Minimum preview times required to prevent rollover; corrective steering maneuver #2.

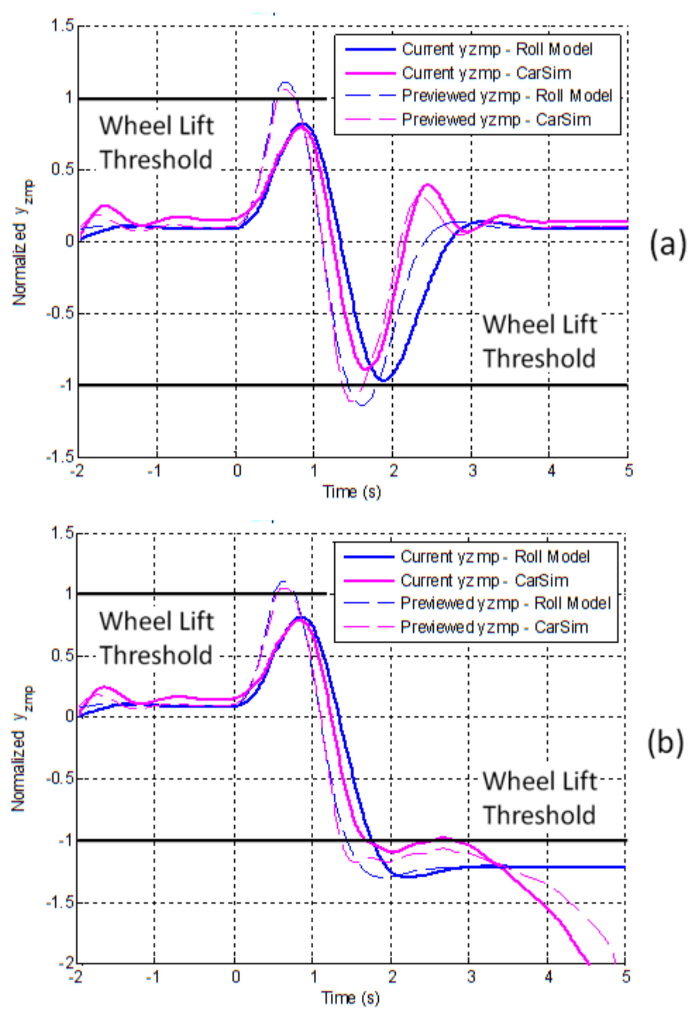

Figure 4.9: y_{ZMP} (a) with and (b) without corrective steering maneuver #2.

and frequency to prevent rollover while best maintaining path-following. It should also be noted that tire lag dynamics were not considered in the vehicle model for these simulations. The effect of tire lag on the preview time needed to prevent rollover is now explored.

4.6 Tire Lag Effects on Rollover Prevention

When considering vehicle rollover, it is important to consider the effects of tire lag. This is especially true for corrective steering maneuvers, as the vehicle does not respond as quickly to changes in steering. Therefore, the simulations performed in Section 4.5 were repeated for the roll model with tire lag dynamics included. Tire relaxation values of 0.7 m and 0.23 m were used for the front and rear tires, respectively.

As foreshadowed previously in the report, initial simulations showed that the infinite series in the previewed input coefficient, B_d, converged too slowly to be applied to the tire lag model. This was due to the fact that the modified terms in the state-space matrices had values several orders of magnitude larger than the matrices that did not include tire lag. Further testing showed that this also occurred for large preview times, even in the model without tire lag.

To address this problem, an alternate method [11] calculated the B_d matrix of Equation 4.23 in discretized form with small time steps, τ, added up to the preview time in the form

$$B_d = \sum_{m=0}^{n-1} (A_d^{n-1-m}) * B\tau \tag{4.32}$$

where $n = T/\tau$. If the chosen time steps are small enough (a value of 0.001 sec was used for this research), Euler approximation of A_d can be used such that Equation 4.32 becomes

$$B_d = \sum_{m=0}^{n-1} [(I + A\tau)^{n-1-m}] * B\tau \tag{4.33}$$

Equation 4.33 provides a more robust solution for the previewed input coefficient and allows the vehicle models with tire lag to be utilized.

The results of the rollover simulation, with tire lag dynamics included, showed that the preview time needed to prevent rollover only increased by approximately 0.01 - 0.02 sec. This increase in preview time occurred for all steering combination inputs and for both corrective steering maneuvers. Therefore, the maximum required preview time for all conditions tested was 0.67 sec, as opposed to 0.66 sec when tire lag was not included.

The influence of tire lag on the dynamics of the vehicle is dependent on the longitudinal velocity. Tire lag effects become less important as the speed of the vehicle is increased. This is an intuitive relationship; as the tires revolve faster, they are able to generate lateral force more quickly from steering changes. Thus, at slower speeds, the effects of tire lag become more pronounced. To this end, simulations were performed to determine the preview times for various longitudinal velocities. Only the steering input that resulted in the maximum preview time (magnitude of -23 deg; frequency of 0.2 Hz; corrective steering maneuver #1) was simulated. The preview times needed to prevent rollover were compared for the various longitudinal velocities for the roll model with and without tire lag as seen in Figure 4.10.

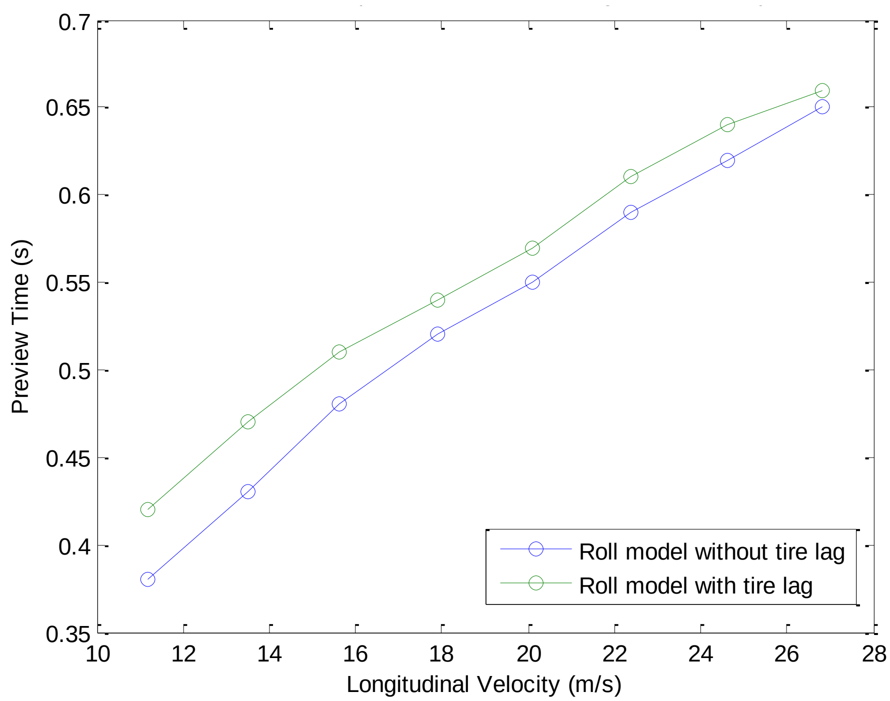

Figure 4.10: Preview times needed to prevent wheel lift for varying longitudinal velocities.

As expected, slightly longer preview times were needed when considering the effects of tire lag. Also as predicted, the need for longer preview times was slightly greater at slower speeds. As speed is decreased, however, the threat of rollover decreases as well. Therefore, when considering rollover at high speeds, it can be seen that the effect of tire lag on the necessary preview time is very small.

4.7 References

[1] S. Lapapong and S. Brennan, “Terrain-aware rollover prediction for ground vehicles using the zero-moment point method,” in *Proc. American Control Conference*, Baltimore, MD, June 2010, pp. 1501–1507.

[2] S. Lapapong, A. A. Brown, and S. N. Brennan, “Experimental validation of terrain-aware rollover prediction for ground vehicles using the zero-moment point method,” in *10th International Symposium on Advanced Vehicle Control (AVEC2010)*, vol. 2, Longsborough, UK, Aug. 2010, pp. 1233–1237.

[3] S. Lapapong, “Vehicle rollover prediction for banked surfaces,” Ph.D. dissertation, The Pennsylvania State University, 2010.

[4] S. Lapapong and S. N. Brennan, “A novel comparative approach to evaluate vehicle rollover propensity,” in *Proc. of 2011 IAVSD*, Manchester, England, Aug 2011.

[5] S. Lapapong, A.A. Brown, K.S. Swanson, and S.N. Brennan, "Zero-moment point determination of worst case maneuvers leading the vehicle wheel lift." in *Vehicle System Dynamics: International Journal of Vehicle Mechanics and Mobility*, vol. 50, sup. 1, pp. 191-214, 2012.

[6] P. Sardain and G. Bessonnet, “Forces acting on a biped robot. center of pressure–zero moment point,” *IEEE Trans. Syst., Man, Cybern. A*, vol. 34, no. 5, pp. 630–637, Sept. 2004.

[7] H. Baruh, Analytical Dynamics. Singapore: McGraw-Hill Book Co., 1999.

[8] A. Dasgupta and Y. Nakamura, “Making feasible walking motion of humanoid robots from human motion capture data,” in Proc. IEEE Int. Conf. on Robotics and Automation, vol. 2, Detroit, MI, May 1999, pp. 1044–1049.

[9] J. Kim and W. K. Chung, “Real-time zero moment point compensation method using null motion for mobile manipulators,” Advanced Robotics, vol. 20, no. 5, pp. 581–593, 2006.

[10] J. L. Meriam and L. G. Kraige, Engineering Mechanics: Dynamics, 4th ed. New York, NY: John Wiley & Sons, Inc., 1997.

[11] B. Kulakowski, J. Gardner, and J. Shearer, Dynamic Modeling and Control of Engineering Systems, 3rd ed. New York: Cambridge University Press, 2007.

Chapter 5 - Conclusions & Future Work

This chapter summarizes the important conclusions found from the work in this thesis. Conclusions are discussed for both the vehicle path following problem and the vehicle rollover problem. The direction of future work in this research is then discussed.

5.1 Vehicle Path Following

For the vehicle path following problem, a closed-loop steering controller developed by MacAdam was implemented. This controller was evaluated at different preview times and road conditions to determine its effectiveness. The two-degree-of-freedom bicycle model was used as the vehicle model and the parameters for a modified 1989 GMC 2500 pick-up truck were used in simulations.

The results of a standard lane change simulation showed that the MacAdam controller performed fairly well up to preview times of 1.0 sec. Even at this preview time, the vehicle was able to follow the road well enough to remain within the bounds of the lane. This was true even after the inclusion of a severe terrain bank angle on the road.

5.2 Vehicle Rollover

For the vehicle rollover problem, the concept of the Zero-Moment Point (ZMP) was introduced and implemented as a rollover metric. Previewed information about the location of the ZMP was then used to identify impending rollover in the future during worst-case driving scenarios and steering inputs. Using this information, corrective steering maneuvers were executed in simulations to mitigate the threat of rollover and determine the minimum preview time needed to prevent wheel lift. The three-degree-of-freedom roll model was used as the vehicle model and the parameters for a modified 1989 GMC 2500 pick-up truck were used in simulations.

The results of the simulations showed that for the worst-case steering input, a minimum preview time of 0.67 sec was needed to prevent wheel lift. It is suggested that a preview time of 0.75 sec be used as a baseline for further study to encompass a wider variety of driving situations and provide a more conservative system.

5.3 Future Work

There are several directions that future research could take in this area. One option is to combine the path following and rollover problems into a closed-loop model. Research could then be done optimizing the controller steering input, and thus vehicle trajectory, to prevent both lane departure and rollover. A situation such as this may occur if an autonomous vehicle detects an obstacle ahead of its path. The system would then need to determine the optimal steering input to avoid the object and stay on the road, all while preventing the vehicle from rolling over. It may also prove useful to investigate the use of yaw rate trajectory as a reference signal rather than lateral position. Using yaw rate would prevent the controller from overriding the driver in determining the future path of the vehicle.

Another option for future work would be to employ Model Predictive Control (MPC), as opposed to the MacAdam controller, in the system. MPC uses a receding horizon technique, making it a more iterative approach than fixed point preview of the system. An approach such as this would provide greater accuracy in the previewed vehicle states and result in a more robust controller.

A third option for future work would be full-scale vehicle testing of the MacAdam model and corrective steering maneuvers. The 1989 GMC 2500 pick-up truck used in the simulations is available at the Penn State test track. Previous work by the research group has automated the truck to be used for rollover testing. Obtaining experimental results is critical in validating the approaches used in this research. These tests would also undoubtedly reveal potential concerns that are unable to be addressed when performing simulations.

ACADEMIC VITA

Paul Stankiewicz

512 Northlawn Drive
Lancaster, PA 17603
717-917-3694
pgs5031@gmail.com

Education

B.S., Mechanical Engineering, 2013, The Pennsylvania State University, University Park, PA

M.S., Mechanical Engineering, 2015 (expected), The Pennsylvania State University, University Park, PA

Honors and Awards

- College of Engineering Graduate Fellowship, The Pennsylvania State University, 2013
- Louis A. Harding Memorial Scholarship, The Pennsylvania State University, 2012-2013
- Dean's List, The Pennsylvania State University, 2009-2013
- Schreyer Honors College Academic Scholarship, The Pennsylvania State University, 2009-2013

Association Memberships/Activities

- Engineers Without Borders, 2011-2013
- American Society of Mechanical Engineers, 2010-2013
- National Society of Collegiate Scholars, 2009-2013

Professional Experience

- Penn State Vehicle Dynamics Research Group, Research Assistant, 2011-2013, University Park, PA
    - Worked under Dr. Sean Brennan; researched methods to predict and prevent vehicle rollover; performed crash testing of anti-ram devices for U.S. embassies as protection against terrorist attacks
- The Boeing Company, Engineering Intern, 2012, Seattle, WA
    - Worked in 737/757 struts, mounts, and fairings group designing specialized repairs for aircraft damage beyond the acceptable limits
- Enviroscan, Inc., Research Assistant, 2008-2010, Lancaster, PA
    - Performed field tests of RASCAN holographic radar to determine functionality in different mediums

Teaching Experience

- The Pennsylvania State University, Mechanical Design & Methodology Teaching Assistant, 2012-2013

Publications

- Stankiewicz, P., Brown, A., Brennan, S., (2013). Determination of Minimum State Preview Time to Prevent Vehicle Rollover. *ASME Dynamic Systems and Control Conference,* (to be published October 2013).